Chapter 3

Dye-sensitized nano-crystalline TiO_2 solar cell

3.1 Introduction

Dye-sensitized nano-crystalline (DNC) TiO_2 solar cell [1], a new type of photovoltaic (PV) cell, has drawn much attention among the scientific community as well as the industrial community due to its low-cost, simple fabrication technique and non-toxicity, and has the potential to become an economically viable means for electrical energy production for common consumer use in near future [2]. In this chapter we will introduce this new type of solar cell with some results of our preliminary investigation on this cell fabricated in our lab. However, before going into the details, a brief historical review of this cell seems to be pertinent to understand some of the basic features of this cell.

The interest in semiconductor-liquid junction solar cell (SLJC), commonly known as photoelectrochemical solar cell (PEC), which utilize a solution of redox electrolyte to form a Metal-Schottky type junction at the interface of the semiconductor and electrolyte, got an impetus after the discovery by Fujishima and Honda[3] that water could be splitted into oxygen and hydrogen, and that light could be converted into electrical energy when a TiO_2 electrode immersed in an electrolyte is illuminated with UV light with platinum as the counter electrode. Soon after its discovery, semiconducting TiO_2 electrodes were put under extreme investigation by the scientists for its application to solar energy conversion. The factors which attributed to the popularity of TiO_2 are its extreme stability even in adverse electrolytic media, continuous operating capability without

degradation, and ease of preparation of polycrystalline TiO_2 electrodes[4]. However, despite its favourable physical and chemical properties, its wide band gap, which is around 3 eV, set a low ceiling to the maximum possible efficiency of solar energy conversion. It can be mentioned here that only ca. 3% of natural sunlight (AM2 conditions) can be absorbed by TiO_2 [5].

Different possible ways have been investigated over the decades to improve the light energy conversion by shifting the absorption towards the visible region of the solar spectrum, such as, using a low band gap semiconductor, decreasing the band gap by incorporating foreign elements into TiO_2, and sensitizing the oxide electrode with another low band gap material (e.g., dye). It has been observed that while most of the high band gap semiconductors resist photocorrosion, the low band gap semiconductors though efficient in light energy conversion, get easily corrroded by the minority carriers at the electrode – electrolyte interface. Therefore, attempts have been made to decrease the band gap of TiO_2 by incorporating different metal cations (Cr, Cu, Fe, Mn, V, Al, Ni, Pb, Co, Zn, Pt, Au, Sb) while at the same time retaining its stability [6 - 11]. Although some success has been achieved in decreasing the band gap with some of the metal ions, all the dopants universally decrease the band gap photocurrent, and the solar efficiency often declines [4]. It is supposed that the dopants and/or their associated defect sites apparently act as efficient recombination centers or hole traps [12].

This apparent failure in shifting the absorption spectrum to the visible region and, thereby, increasing the efficiency of TiO_2 based PEC cell, led to the sensitization of TiO_2 by dye molecule with the band gap energy typically in the range of 1.6 - 2 eV which can cover much of the solar spectrum in the visible region [13 - 15]. The dye sensitization phenomenon of semiconductor surface, where light energy smaller than the band gap energy can be absorbed, was first observed more than a century ago and plays a vital role in silver halide photography and photoelectrochemistry, both of which rely on photoinduced charge seperation. Panchromatic film, able to render the image of a scene realistically into black and white, following on the work of Vogel in Berlin after 1873 [16], associates dyes with the halide semiconductor grains. The first reported sensitization of a semiconductor photoelectrode took place about the same time [17]. However, the verification of the operating

mechanism in dye-sensitization that an electron (hole) is injected into the conduction (valence) band by the excited dye molecule adsorbed at the surface of the semiconductor, depending on the band positions of the semiconductor and the energy levels of the dye, dates to 1960's only [18]. This phenomenon has been exploited by the scientists for years as a means to extend the spectral response of photoelectrochemical cells which are based on high band gap materials that are photostable in electrolytic media [13 - 15]. However, the problem of low light conversion efficiency remained since only surface attached species alone can contribute to the photoresponse of the device. Thus at a monolayer coverage of the dye on a flat electrode, though the quantum efficiency of charge injection per molecule of the adsorbed dye approaches unity, the overall efficiency is at most a few percent and thicker layers are found to be electrically insulating that do not contribute to the charge transfer or current generation. A breakthrough in this problem was made by Gratzel and his co-workers [1, 19] by the development of a nano-porous TiO_2 film consisting of nano-meter sized particles where the effective surface area can be enhanced as high as or even more than 1000 times depending on the thickness of the film. When such a film is covered with even a monolayer of dye, light intercepts many particles increasing the light absorption greatly. Because of the close contact between each dye molecule and TiO_2 particles, practically all of the photoexcited electrons could be collected efficiently in this system. Efficiency as high as 10% has been reported for this dye-sensitized nano-crystalline solar cell with the TiO_2 film thickness being around 10 μm [19].

3.2 Basics of a dye-sensitized TiO_2 solar cell

3.2.1 Cell structure

The schematic structure of a DNC cell is shown in Fig. 3.1. Nano-crystalline TiO_2 thin film with crystal size 10-20 nm, supported on a F-doped SnO_2 coated transparent conducting oxide (TCO) glass substrate, is used as a photoelectrode. Typically a thickness of around 10 μm is used for nano-porous nano-crystalline TiO_2 thin film in a conventional DNC cell, giving an effective surface

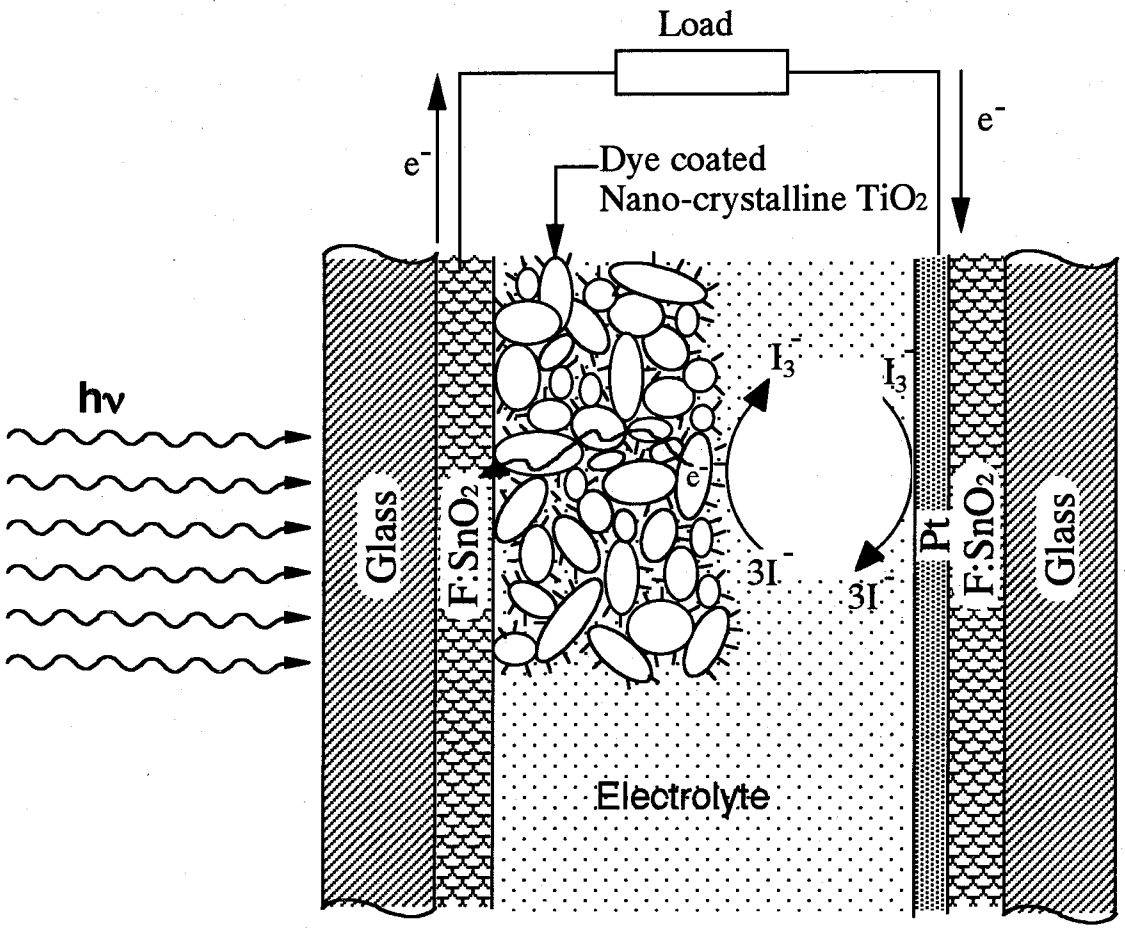

Fig. 3.1 Structure of dye-sensitized nano-crystalline TiO_2 photoelectrochemical solar cell

area which is almost 1000-fold larger than the geometrically projected area. TiO_2 nano-crystals are covered with a mono-layer of light absorbing dye molecules and the pores of the nano-crystals are filled with a liquid electrolyte containing iodide/triiodide (I^-/I_3^-) redox couple in a non-aqueous electrolyte, such as acetonitrile. A transparent platinized conducting glass, placed over the nano-crystalline TiO_2, serves as a counter electrode. The edges of the cell are strongly sealed to preserve the liquid electrolyte.

The cell is usually illuminated from the TiO_2 coated side of the glass substrate. Upon illumination, the photoexcited dye molecules inject electrons into the conduction band of TiO_2. Close necking of the TiO_2 nano-crystals allows smooth percolation of the injected electrons through the film with little loss, which are then collected at the TCO substrate. The collected electrons, after passing through the external circuit and delivering power to the load, re-enters the cell at the counter electrode

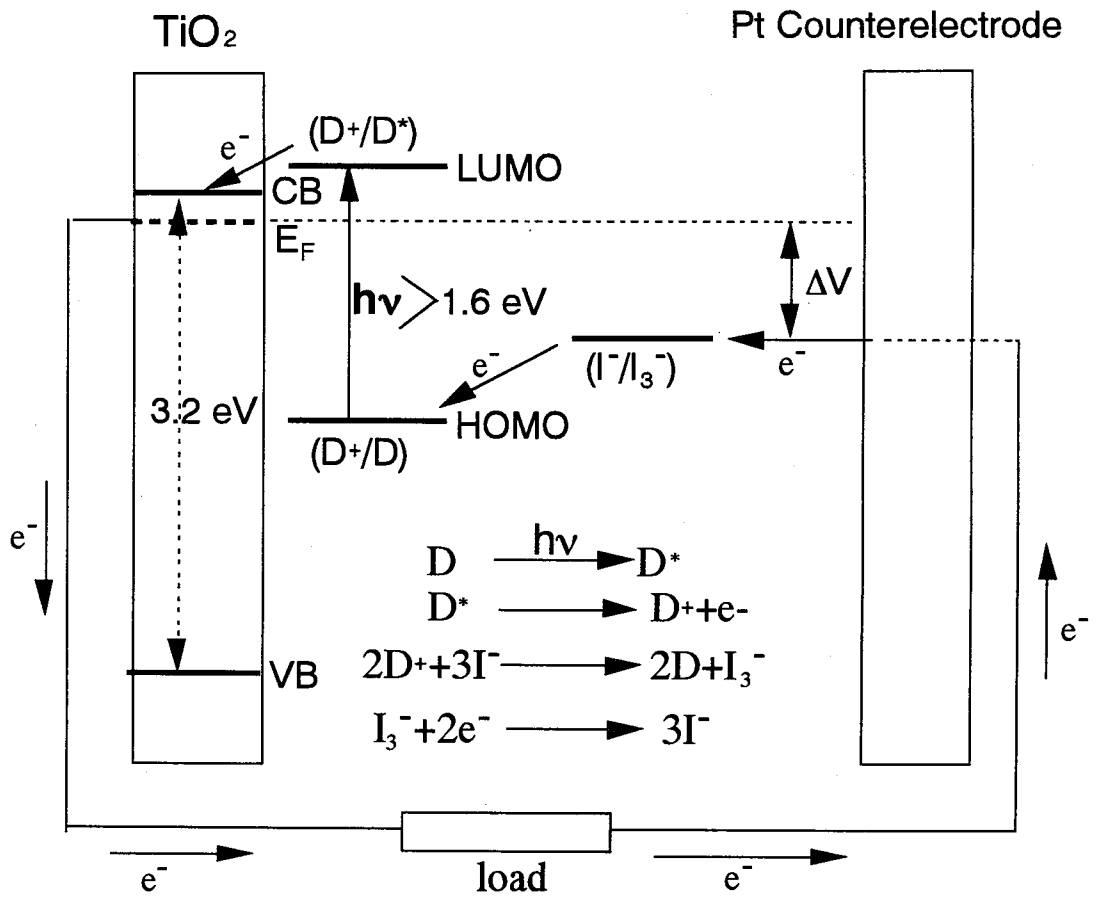

Fig. 3.2 Schematic representation of the working principle of dye-sensitized photovoltaic cell.

and reduce triiodide to iodide. The iodide diffuses into the pores of the TiO_2 film where it oxidizes to triiodide and reduces the photo-excited dye to its original state.

3.2.2 Operating principle

Unlike the solid-state *p-n* junction solar cells, the function of light absorption and charge carrier transport are seperated in a DNC cell; the function of light absorption is performed by a mono-layer of dye absorbed chemically on the semiconductor surface while charge tranport takes place in the nano-crystalline film where the nano-crystals are connected in a fashion producing intimate electronic contact between almost all the perticles constituting the film. A schematic drawing of the energy levels of a DNC cell is shown in Fig. 3.2. The desired pathway for a photoexcited electron in the cell is also indicated.

The dye is excited from its ground state (D) to the excited state (D^*) by the absorption of a

photon where one electron is excited from the highest-occupied-molecular-orbital (HOMO) to the lowest-unoccupied-molecular-orbital (LUMO) of the dye. The excited electron is then injected into the conduction band of TiO_2 as a result of which the dye gets oxidized (D^+) which is then reduced by the iodide/triiodide redox electrolyte to its ground state. As the dye cation accepts an electron from the species I^- of the I^-/I_3^- redox couple in the electrolyte, regenerating the dye, the oxidized redox species I_3^- travels back to the counter electrode where it gets reduced to I^-. The overall equilibrium is maintained by the diffusion controlled migration of the redox species in the solution. The total reaction of the complete process can be described by the following equations:

$$D + h\nu \longrightarrow D^*$$

$$D^* \longrightarrow D^+ + e^-$$

$$\downarrow$$

conduction band of TiO_2

$$D^+ + 3I^- \longrightarrow 2D + I_3^-$$

$$I_3^- + 2e^- \longrightarrow 3I^-$$

$$\uparrow$$

counter electrode

The electrons injected into the TiO_2 conduction band by the dye molecules travel across the nano-crystalline film to the TCO glass support which serves as a current collector. Since the DNC cell is a majority carrier device where current conduction takes place only due to transport of electrons through TiO_2 while the holes remain localized on the oxidized dye molecules, the electron-hole recombination loss in the bulk of the semiconductor is absent in the nano-crystalline TiO_2 solar cell. Thus the requirement of a pure and well-ordered semiconductor material to have a long diffusion length, which is essential for solid-state PV cells, is excluded in the DNC cells. The only recombination that can take place in a DNC is at the semiconductor electrode – electrolyte interface (SEI) where the injected electrons into the conduction band of TiO_2 can recombine with the oxidized dye molecules or the oxidized species in the electrolyte. Fortunately the forward electron injection is an extremely efficient process than the recombination process that occur at the interface. As shown in

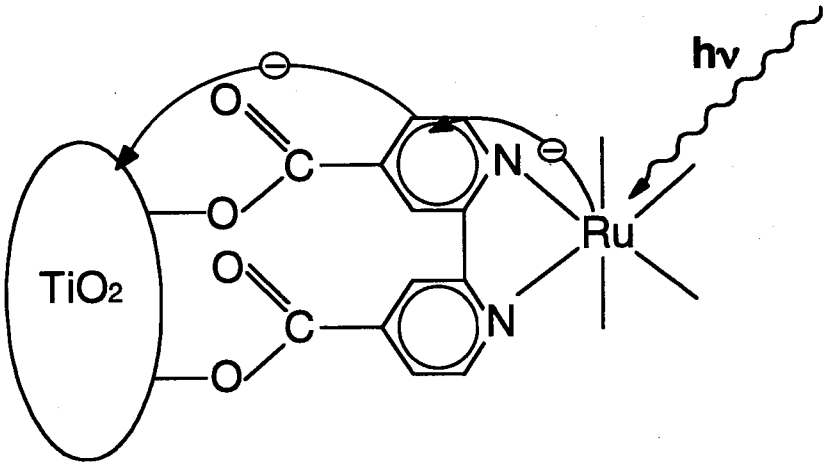

Fig. 3.3 Molecular orbital diagram for ruthenium complexes anchored to the nano-crystalline TiO_2 surface by a carboxylated bipyridyl ligand.

Fig. 3.3, the dye, which is usually a Ru complex ($RuL_2(SCN)_2$), is attached to the TiO_2 surface by the carboxylated bipyridyl ligand. The visible light absorption of these type of complexes is a metal-to-ligand charge transfer (MLCT) process. The carboxylate groups, directly coordinated to the surface titanium ions, establish an intimate electronic coupling between the excited Ru complex and the 3*d* wave function manifold of the TiO_2 film. As a result, the electron injection from the excited sensitizer into the semiconductor is an extremely rapid process occurring in less than a picosecond. On the other hand, the back-reaction of electron with the oxidized dye involves a *d* orbital localized on the Ru metal whose electronic overlap with the conduction band of TiO_2 is small, rendering the back-transfer process almost three orders of magnitude slower than the forward injection process. The details of the operation mechanism and charge transfer kinetics of a DNC cell can be found from literature [20 - 24].

The photovoltage, ΔV, of a nano-crystalline solar cell represents the difference between the Fermi level of titanium dioxide under illumination and the redox potential of the electrolyte (Fig. 2.2). Using the triiodide/iodide redox couple, under full sunlight an open-circuit voltage of $0.7-0.9$ V can be measured. Very high incident monochromatic photon-to-current convesion efficiency, exceeding 75%, has been obtained for these cells which, when corrected for reflection and absorption losses because of the TCO glass substrate, yeilds a value of almost 100%. With $RuL_2(SCN)_2$ as a

dye-sensitizer, and under an illumination of 1 sun at AM 1.5 condition, short circuit current of 18.3 mA/cm^2, open circuit voltage of 0.72 V and a fill factor of 0.73 have been obtained which yeilds an overall efficiency of around 10% [19]. The energetics of all the three components (the semiconductor, the dye, and the electrolyte) in Fig. 3.2 can be varied for optimal matching with regards to the charge transfer and output voltage. Large efforts have already been made to synthesize new dyes for better spectral overlap with the solar spectrum and to find an alternative to the I^-/I_3^- redox couple to increase the output voltage [19, 25]. A new black dye (4,9,14-tricarboxy 2,2'-6,6'-terpyridyl ruthenium (II) trithiocyanate) has recently been reported by Gratzel that gives an efficiency of around 11% [26]. However, no better candidate to substitute I^-/I_3^- redox couple, which must be efficient in dye interception and electron uptake at the counter electrode, has been found to minimize the loss of photovoltage (~ 0.4 V) due to the large difference between the I^-/I_3^- redox potential and the HOMO of the dye molecule.

As already mentioned in section 1.4 of chapter 1, though many groups are working on DNC cell to reproduce the 10 % efficiency as originally reported by Gratzel, the success is limited to only 6 - 7 %. Therefore, a careful and systematic study of various components and parameters of the DNC cell and their effect on cell performance is essential before one can reproduce the original cell. Beside investigating the solid-state aspect of TiO_2 solar cell, we have also made some preliminary study on the DNC cell, which is concentrated mainly on the TiO_2 film preparation and its effect on the cell performance when prepared under different conditions. Thin TiO_2 films with thickness around 1 μm are used in our experiment which are ten times less thinner than the thickness used in the original Gratzel cell (10 μm) and this results in a transparent cell with an efficiency of around 1.45 % under 1 sun AM1.5 conditions. Details of the experimental procedure and results are described in the following sections.

3.3 Experimental

In the course of time, sol-gel method has evolved as a mature and convenient technology to prepare nano-crystalline TiO_2, both in thin film form as well as in powder form, for various optical and opto-electrical applications. Two processing routes to prepare the nano-crystalline TiO_2 film for solar cell application have been reported in the literature. In the first approach, particles are applied to a conducting glass substrate from a suspension by screen printing or spraying or spreading using a glass rod, and then dried and sintered to form electrical contact between the particles [27]. In the second approach, nano-crystalline particles are directly formed onto the substrate by electrochemical or chemical deposition process[28]. Sol-gel dip-coating is used as a second approach where the sol is prepared by carrying out hydrolysis of titanium alkoxide in alcoholic solution and then the film is deposited by dipping the substrate into the sol and pulling it up at a constant speed. We have adopted both the routes, namely, spreading of colloidal sol by a glass rod and sol-gel dip coating method, to prepare the films. In the glass rod spreading method, we have studied the effect of triton-X addition to the colloidal sol of TiO_2 on the film surface morphology and cell performance. Triton-X, which is a kind of detergent and has a boiling point of around 110 °C, is usually added to the colloidal sol of TiO_2 to assist the spreading of the sol on the substrate. In the dip-coating method, we have studied the effect of pulling speed on the cell performance. In the following sections we will describe the details of the DNC cell preparation which includes TiO_2 thin film preparation, dye-adsorption onto the TiO_2 film, and final assembling of the cell (electrolyte injection and sealing).

3.3.1 TiO_2 thin film preparation

(1) Glass rod spreading method

Sol of colloidal nanocrystalline TiO_2 (conc. 5.2 wt.%, particle size 10-20 nm) was used as received. Triton-X was added to the sol at an amount of 0, 0.25, 0.5, 0.75, and 1.5 vol.% and stirred using a magnetic stirrer for about 30 minutes to have a homogeneous mixture. TCO glass substrates (Solaronix, FTO8) with a thickness of 3 mm and sheet resistance of 8 Ω/□, were used to deposit the

films. Before deposition, the substrates were cleaned in acetone and methanol using an ultrasonic cleaner and ethched with 10% aqueous HF solution for 10 sec. Two edges of the TCO substrate were covered with scotch tape (3M, thickness 50μm) that serve as a frame and spacer, and also cover some portion of the TCO for making electrical contacts. A drop of colloidal TiO_2 sol was placed in the space between the two tapes and was spreaded evenly by a glass rod. The film was then dried at 80 ℃ for around 10 min, tapes were removed and finally the film was subjected to heat-treatment at 450 ℃ for 30 min. Film of thickness of around 1 μm with slight variation over different regions has been obtained by this method, measured by a step profilometer. The thickness can be further varied by making repeated coatings, or by changing sol concentration, or by changing the thickness or the number of layers of the scotch tape.

(2) Sol-gel dip-coating method

Nanocrystalline TiO_2 thin films were also deposited on the same TCO glass substrate (Solaronix, FTO8) by using sol-gel dip-coating method. Very thin transparent films of TiO_2 on large substrate can be deposited using this method which will be useful for window application. The details of the sol solution preparation and film deposition procedure are same as those described in section 2.2 of chapter 2. The rate of pulling speed was varied from 0.1 mm/s to 0.5 mm/s. All the films were dried at 80 ℃ for 10 min and heat-treated at 450 ℃ for 30 min after each coating, and were coated for 10 times to get a film thick enough for solar cell application.

3.3.2 Dye-adsorption

The dye (Ruthenium 535 bis-TBA), *cis*-bis(isothiocyanato)bis(2,2'-bipyridyl-4,4'-dicarboxylato)-ruthenium(II)bis-tetrabutylammonium, purchased from Solaronix, was used as received. The dye was dissolved in dry ethanol at a concentration of 0.2 g/l. Nanocrystalline TiO_2 thin films deposited on TCO substrates were kept immersed in the dye solution for 2 h at 60 ℃ in a water bath for dye adsorption. To minimize rehydration of the TiO_2 surface from moisture from the ambient air, which causes the dye to desorb and degrades the cell performance, the TiO_2 electrodes, while still

warm (80 – 100 °C) from annealing, were immersed in the dye solution. After dye adsorption, dye-coated films were rinsed in dry ethanol, dried by blowing N_2 stream and were kept in a air tight case in a dark place till the assembling of the cell.

3.3.3 Assembling of dye solar cell

Two narrow strips (~2 mm) of sealing material, Amosil-4, purchased from Solaronix, were placed on the two sides of the TiO_2 film and the counter electrode, which is a platinized SnO_2 coated glass, was placed on top of the TiO_2 film and the two electrodes were clamped tightly together. The module was left over for 24 h at room temperature to cure the sealant. After this a small drop of redox eletrolyte was put on the top of one of the open edges whereby the elctrolyte is soaked up in the inter-electrode space by capillary action. The redox electrolyte used (Iodolyte GD-50) was purchased from Solaronix, which is based on purified glutaronitrile, a high boiling point solvent and contains 50 mM triiodide and saturated anhydrous lithium iodide. The excess of electrolyte was wiped off from both the open edges which were then cleaned carefully with acetone (usually electrolyte is more soluble in acetone than in alcohol) to remove any remaining trace of electrolyte. The open edges were sealed by the sealant, Amosil-4, and the cell was left over for another 24 h at room temperature to let the sealant dry. Electrical connections to the cell was made by attaching copper wire onto the TCO substrate by silver paste.

3.3.4 Characterization

Surface morphology of the films were observed by an optical microscope and a high resolution scanning electron microscope (SEM). Thickness of the films was measured by a step profilometer and also from SEM cross-sectional view. Current-voltage (I-V) characteristics of the cells, both under dark and illumination (1 sun AM 1.5 conditions), were recorded using a solar simulator. Quantum efficiency (spectral dependence of photon-to-current conversion efficiency) and UV-visible transmission spectra of the DNC cells were also recorded.

3.4 Results and discussion

3.4.1 Glass rod spreading method

3.4.1.1 Surface morphology

Figure 3.4 shows the surface morphology of the TiO_2 thin films deposited on conducting glass substrate from colloidal TiO_2 sol containing different amount of triton-X. As it can be observed from these photographs, for the film which is prepared from the sol that contains no triton-X, heavy crack formation takes place. With the addition of slight amount (0.25 vol %) of triton-X, essentially smooth film surface has been obtained. Gradual increase in the amount of triton-X shows that while there is not much difference between the films that are prepared with 0.25 and 0.5 vol % of triton-X, further increase in the amount of triton-X causes crack formation which increases both in size and in number with the increase in the amount of triton-X. Being a detergent triton-X, when a small amount of it is added to TiO_2 colloidal sol, assist in spreading the sol on the substrate and, thereby, the formation of a smooth surface. However, most probably, excess amount of triton-X addition results in the agglomeration of triton-X at different places of the film, which when starts evaporating (boiling point around 110 °C) during heat-treatment exerts high pressure at those specific places of the filmand results in crack formation.

SEM micrographs of the films that are prepared from the sol containing 0.0, 0.25 and 0.75% of triton-X are shown in Fig. 3.5. For both the cases, i.e., with and without triton-X, films have the porous structure. However, for the film which is prepared using the sol that contains no triton-X, film is less porous and the TiO_2 particles are more closely clustered than the films that are prepared with triton-X addition. However, not much difference in the surface morphology can be observed from these SEM pictures for films with 0.25 and 0.75 vol % of triton-X addition. From these figures, it can be concluded that when no triton-X is added to the sol, particle agglomeration takes place resulting in crack formation as observed in Fig. 3.4. Slight addition of triton-X to the sol resists particle agglomeration, assists in uniform spreading of the particles over the substrate and, thereby,

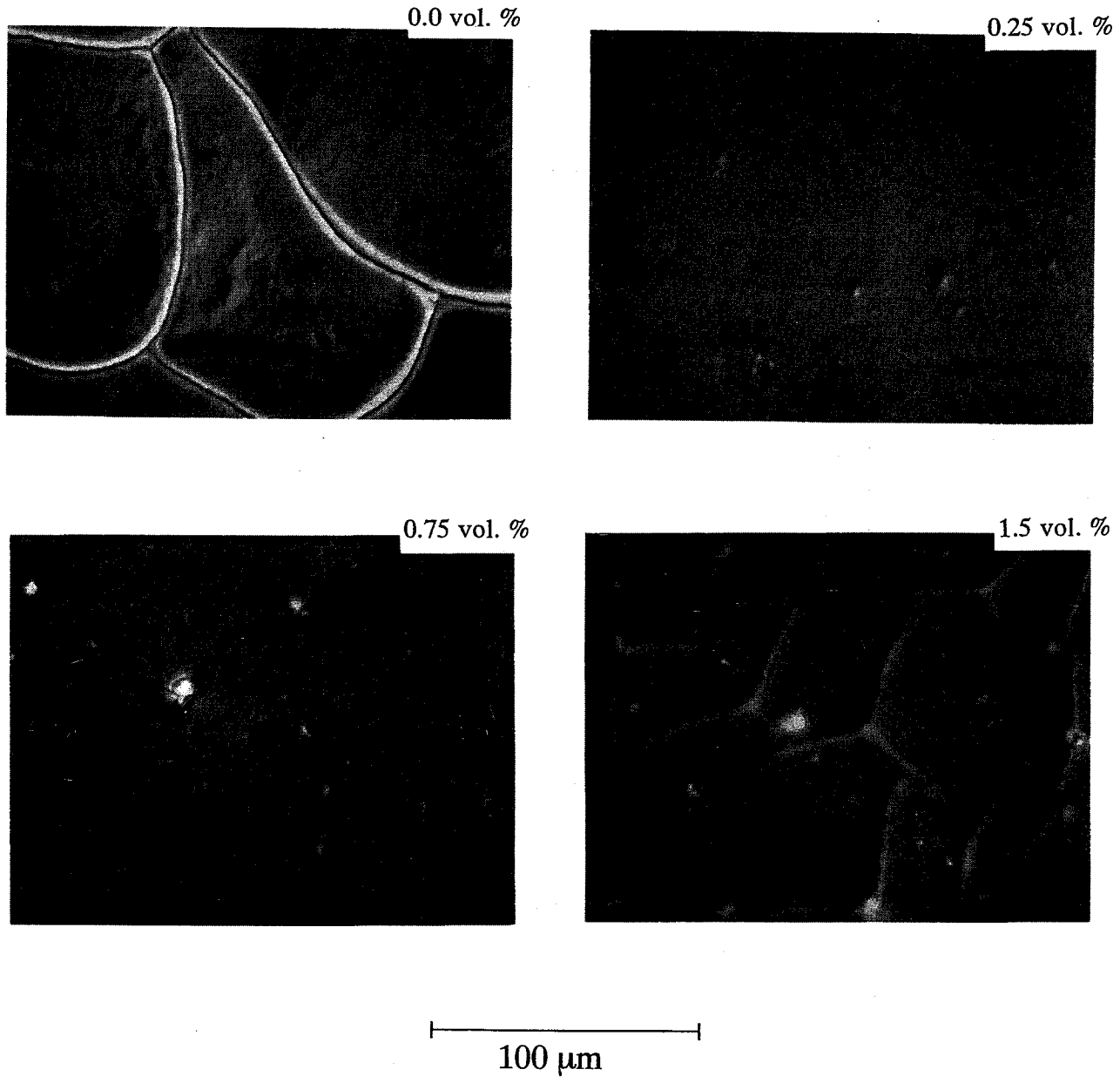

Fig. 3.4 Surface morphology of the TiO_2 thin films deposited on SnO_2 coated glass substrate using colloidal TiO_2 sol containing different amount of triton-X, by optical microscope.

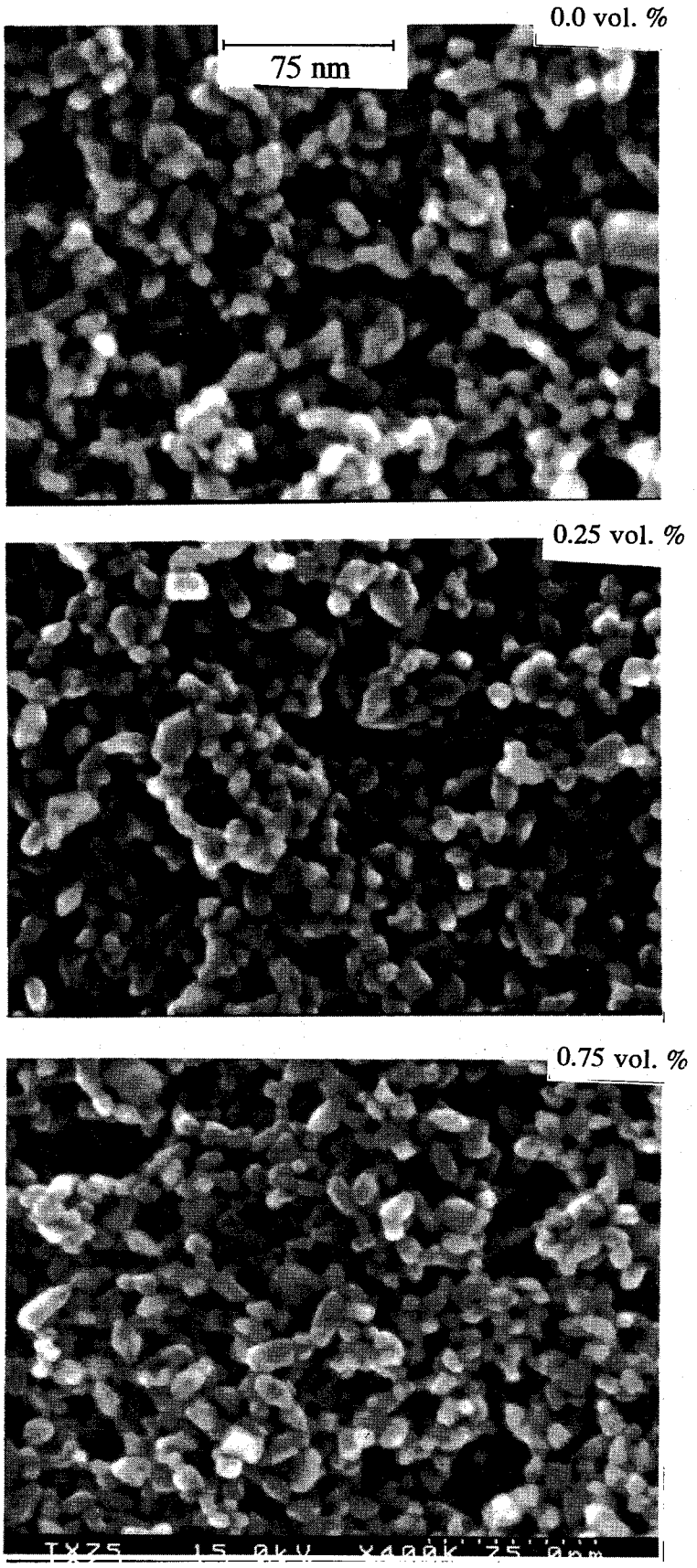

Fig. 3.5 SEM surface morphology of the TiO_2 thin films deposited on SnO_2 coated glass substrate using TiO_2 colloidal sol containing 0.0, 0.25 and 0.75 vol % of triton-X.

helps in the formation of a smooth surface of high porosity.

3.4.1.2 $I-V$ characteristics

The $I-V$ characteristics of two DNC cells, one prepared using the TiO_2 film with no triton-X and the other with 1.5 vol % of triton-X being added to the sol, measured under 1 sun at AM 1.5 illumination, are shown in Fig. 3.6. The cell with no triton-X being used in the film, shows an efficiency of only 0.26%, while the cell with triton-X (1.5 vol %), shows an efficiency of around 1.2%. While there is a small decrease in the open-circuit voltage, the short-circuit current is increased by almost 5 times. Two main reasons for this big difference may be that the formation of large cracks and agglomeration of particles in the TiO_2 film, as observed in the optical and SEM pictures, both of which decrease effective surface area of the film and thereby reduce the photocurrent. Further, the large cracks and the big clusters act as scattering centers and may reduce the absorption of incident light in the cell.

Figure 3.7 shows the dark $I-V$ characteristics of the DNC cells with the TiO_2 films being prepared from TiO_2 sols containing different volume% of triton-X. While the DNC cells work on the principle of photo-electrochemical cell, their photovoltaic performance in terms of solar energy conversion and $I-V$ characteristics are comparable to those of solid-state $p-n$ junction solar cells. Similar to $p-n$ junction diode, the $I-V$ characteristics show rectifying characteristics. However, the cut-in voltage is not well defined and the current increases slowly rather than exponentially at relatively lower voltages which may be due to presence of different surface states in nano-crystalline TiO_2. At higher voltages, where the increase in current is rather sharp, the deviation from the exponential increase is mainly due to the resistance caused by the TiO_2 film as well as that by the SnO_2 conducting layer. The slope of the straight line portion of the curve will give the total resistance faced by an electron as it travels through the cell. Since all other parameters are fixed, the variation in the resistance obtained by this method will merely represent the variation in the resistance of the TiO_2 film itself. Figure 3.8 shows the variation in the cell resistance with the vlume % of triton-X added to the

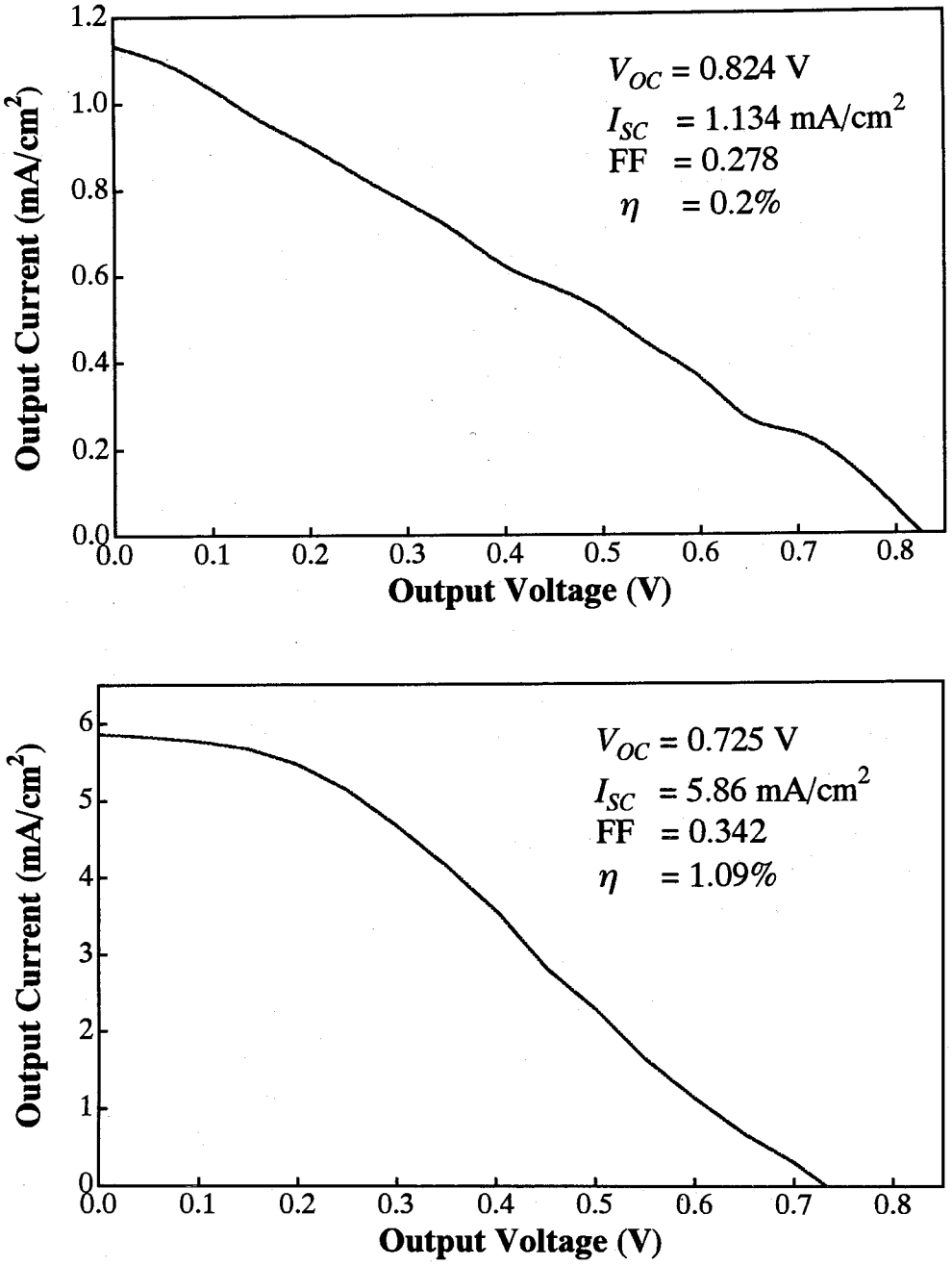

Fig. 3.6 *I-V* characteristics of dye-sensitized TiO_2 solar cell, under 1 sun AM 1.5 illumination, using the TiO_2 films prepared from the TiO_2 colloidal sol; (top) without addition of triton-X and (bottom) with 1.5 vol % of triton-X addition to the TiO_2 sol.

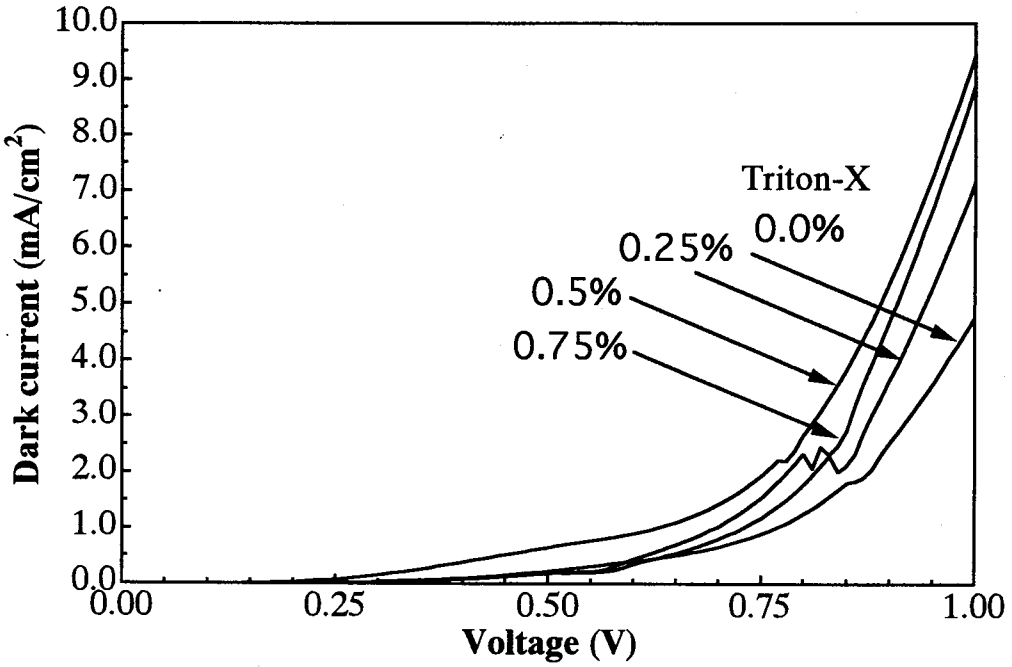

Fig. 3.7 Dark *I-V* characteristics of DNC cells with the TiO_2 films prepared from TiO_2 sols containing different volume % of triton-X.

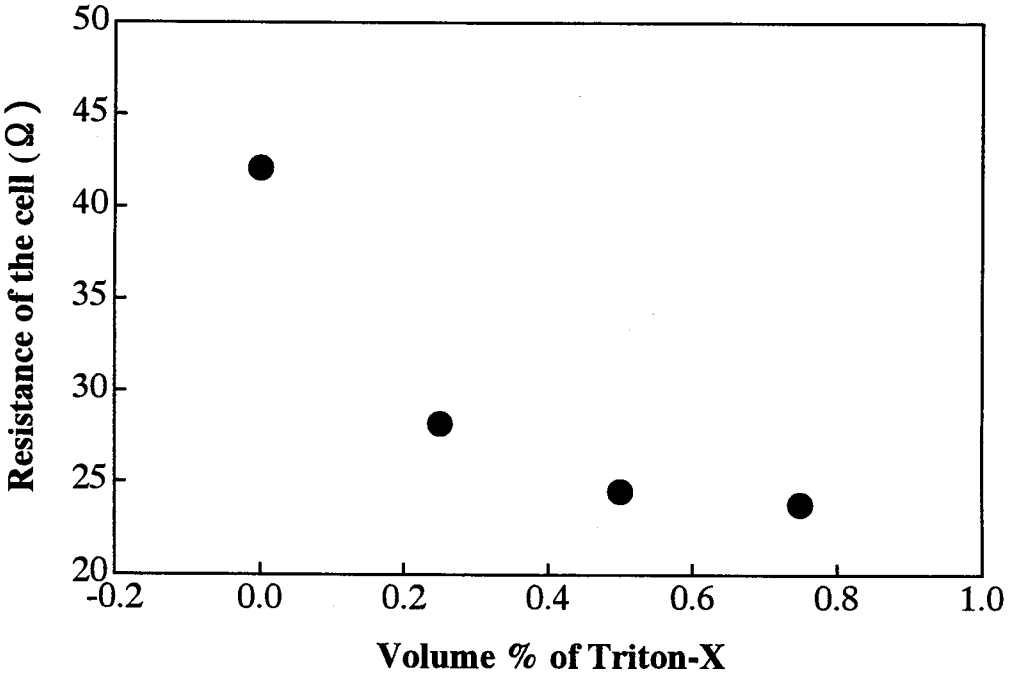

Fig. 3.8 Variation in the cell resistance with triton-X added to the TiO_2 sol, calculated from the slope of the straight line portion of the *I-V* curves in Fig. 3.7.

TiO_2 sol, which is calculated from the slope of the straight line portion of the dark $I-V$ characteristics in Fig. 3.7. For the cell with no triton-X, the cell resistance is very high. However, slight addition of triton-X decreases the cell resistance by a significant portion and further increase in triton-X gradually leads to a saturation in the cell resistance. It can be concluded from this result that for the film without triton-X, though the particles are clustered together in small small groups (Fig. 3.5), the overall contact between all the particles from film surface to the TCO layer is very poor. Addition of triton-X helps spread the particles uniformly leading to better contact among the individual particles as well as all the particles constituting the film.

The dependence of open-circuit voltage V_{OC}, short-circuit current I_{SC}, efficiency and the fill factor (FF) on the triton-X content, obtained from the $I-V$ characteristics measured under illumination at 1 sun AM1.5 conditions, are shown in Fig. 3.9. The open-circuit voltages obtained are quite high and is highest (0.824 V) for the cell without triton-X. Further, V_{OC} gradually decreases with addition of triton-X upto 0.5 vol % after which it increases slightly. The reason for this variation of V_{OC} with triton-X is not clear at this stage. There is a big increase both in I_{SC} and efficiency, from 1.2 mA/cm^2 and 0.2% for the cell with no triton-X (not shown in the figure) to 5.9 mA/cm^2 and 1.09% for the cell with slight addition of triton-X. I_{SC} is found to increase upto 0.75 vol. % of triton-X addition after which it decreases slightly. The increase in I_{SC} upto 0.75 vol. % of triton-X is attributed to the better film porosity, i. e., increased surface area (Fig. 3.5) and lower resistance of the film, i.e., better contact among the particles due to addition of triton-X. The decrease in I_{SC} after this may due to reformation of cracks as observed in Fig. 3.4. Maximum cell efficiency (1.45%) has been obtained with 0.5 vol. % of triton-X addition which decreases slightly with further increase in triton-X. The FF for the cell without triton-X is very low, only 0.278, which is probably due to the high siries resistance of the cell (Fig. 3.8). Maximum FF has also been obtained for the cell with 0.5 vol % of triton-X addition. It can be mentioned here that surface morphology of the film with 0.5 vol % of triton-X addition by optical microscope revealed similar smooth structure as that observed for the film with 0.25 vol % of triton-X addition (Fig 3.4) and shows the best cell performance in terms

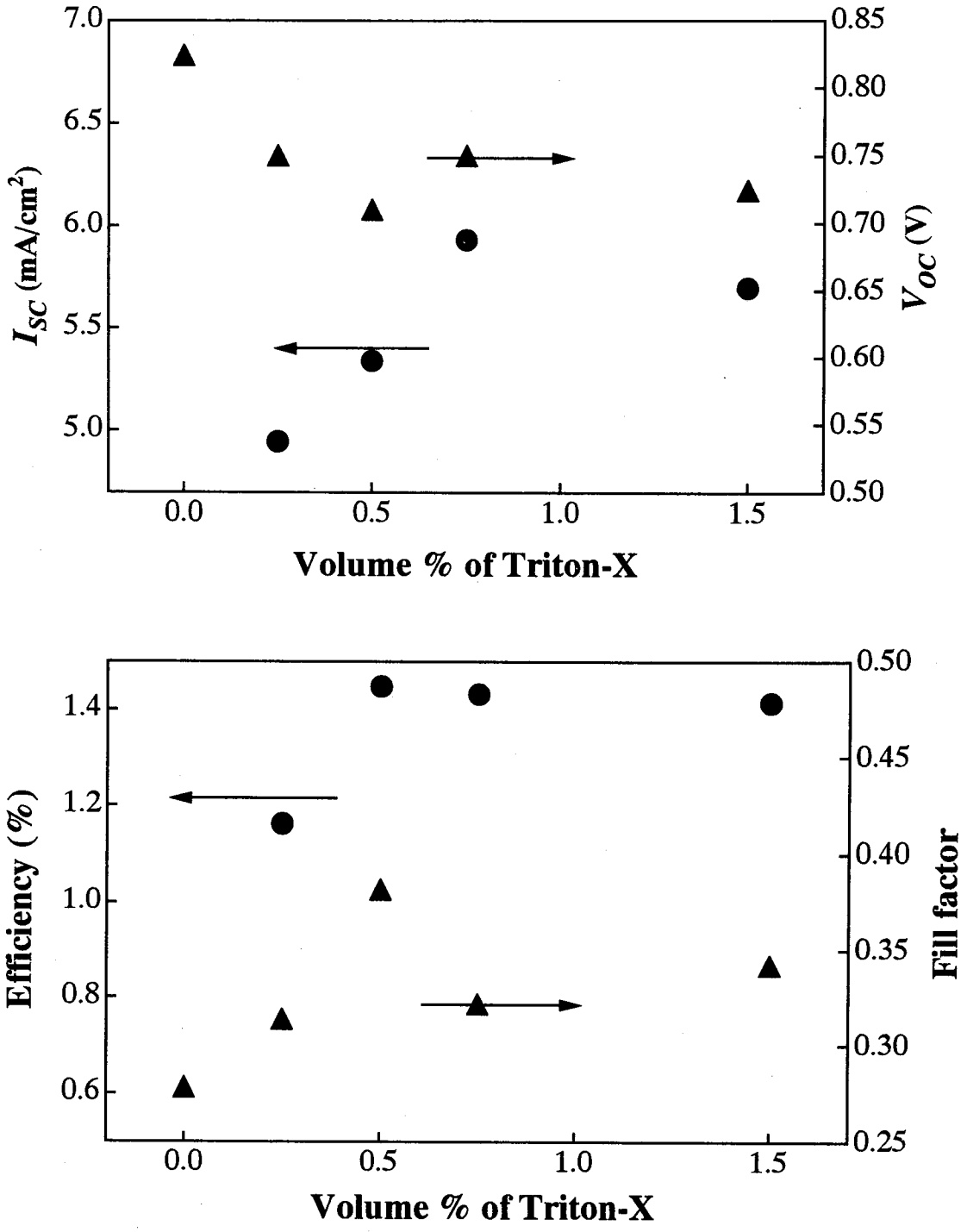

Fig. 3.9 Dependence of open-circuit voltage V_{OC}, short-circuit current I_{SC}, fill factor (FF) and efficiency of the DNC cell on the vol. % of triton-X added to the TiO_2 sol.

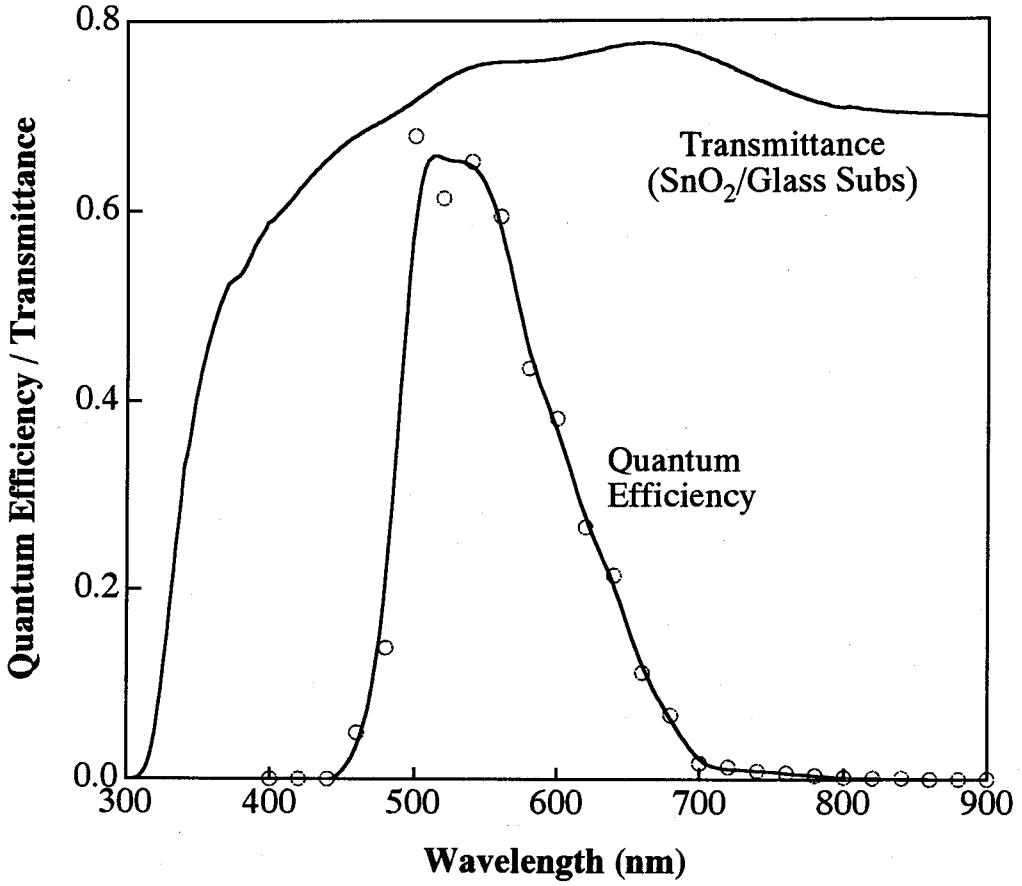

Fig. 3.10 Quantum efficiency and transmission plots of dye-sensitized nanocrystalline TiO_2 solar cell as a function of light wavelength, prepared by using TiO_2 colloidal sol with triton-X 1.5 vol%. Film thickness is about 1 μm.

of efficiency and fill factor. From these results it can be concluded that the best performance of a cell can be obtained with maximum amount of triton-X addition for which no crack formation takes place.

3.4.1.3 Quantum efficiency

Quantum efficiency (Q. E.) spectrum a DNC cell, which shows the spectral dependence of incident photon-to-current conversion efficiency, together with the transmission spectrum of the bare TCO glass substrate, is shown in Fig. 3.10. The Q. E. spectrum, which is in the wavelength range of 450 to 700 nm, is relatively narrower than that reported by Gratzel's group (450~800 nm) where they have used the same dye. This may be due to the fact that in our cell the TiO_2 film thickness is only around 1 μm which is much less than that (10 μm) used in the DNC cell reported by Gratzel's group. Since the photons of longer wavelength have lower absorption probability by the dye than those of

shorter wavelength, the longer wavelength photons get easily transmitted through the film before they can be absorbed by the dye which makes the Q. E. spectrum to shift from 800 nm to around 700 nm. The maximum photon-to-current conversion efficiency obtined is 68% at 500 nm which when corrected for refletion and absorption losses by the substrate yields nearly 95 % Q. E. since only 72% of the total light energy can be passed through the TCO substrate at this wavelength as can be observed from the transmission spectrum.

3.4.2 Sol-gel dip-coating method

Sol-gel dip-coating method is a popular way to deposite various oxide films for diverse optical and electro-optical applications. One major advantage of this technique is this that films can be deposited on large substrate while different parameters like film thickness, particle size and porosity, etc. can be controlled to a good approximation by suitable adjustment of different deposition conditions. Very thin (few tens of nm to several 100 nm) and highly transparent films of TiO_2 on large substrate can be deposited by this method which can be used to develop transparent or semi-transparent DNC cells suitable for window application. Since both sides of the substrate get

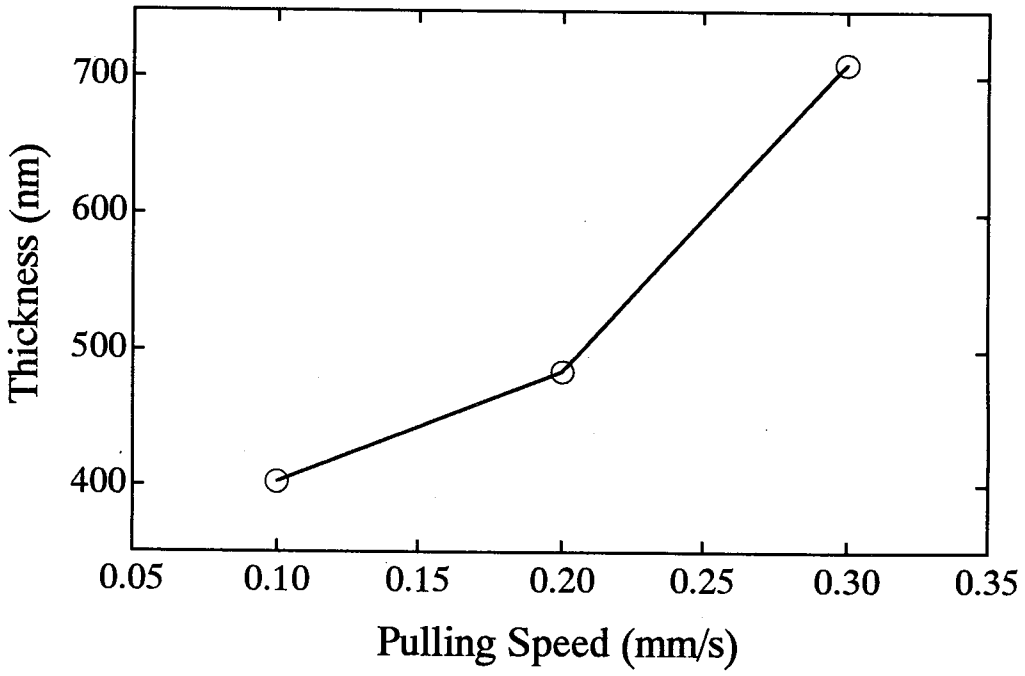

Fig. 3.11 Dependence of TiO_2 film thickness on the pulling speed in the dip-coating method.

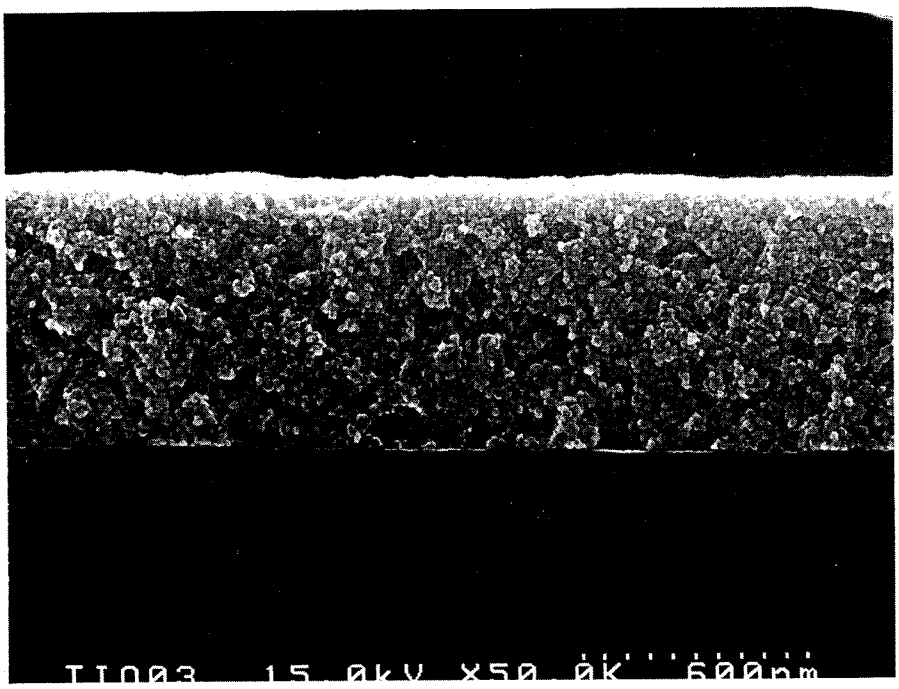

Fig. 3.12 SEM cross-sectional view of a TiO_2 film deposited at a pulling speed of 0.3 mm/s by sol-gel dip-coating method.

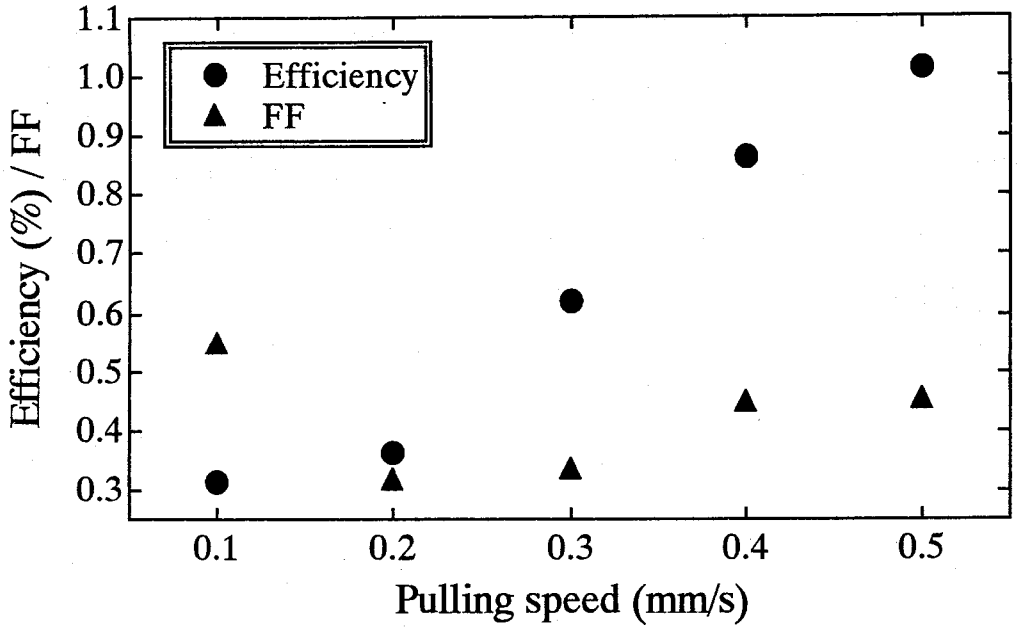

Fig. 3. 13 Dependence of efficiency and fill factor of DNC cell on pulling speed in the sol-gel dip-coating method used to prepare TiO_2 film.

coated with this method, it is postulated that while the film on one side can be used for the DNC cell fabrication, the other side can be used for air purification, if used in the window of a building. We have deposited TiO_2 films using this method by varying the pulling speed. The thickness of the films

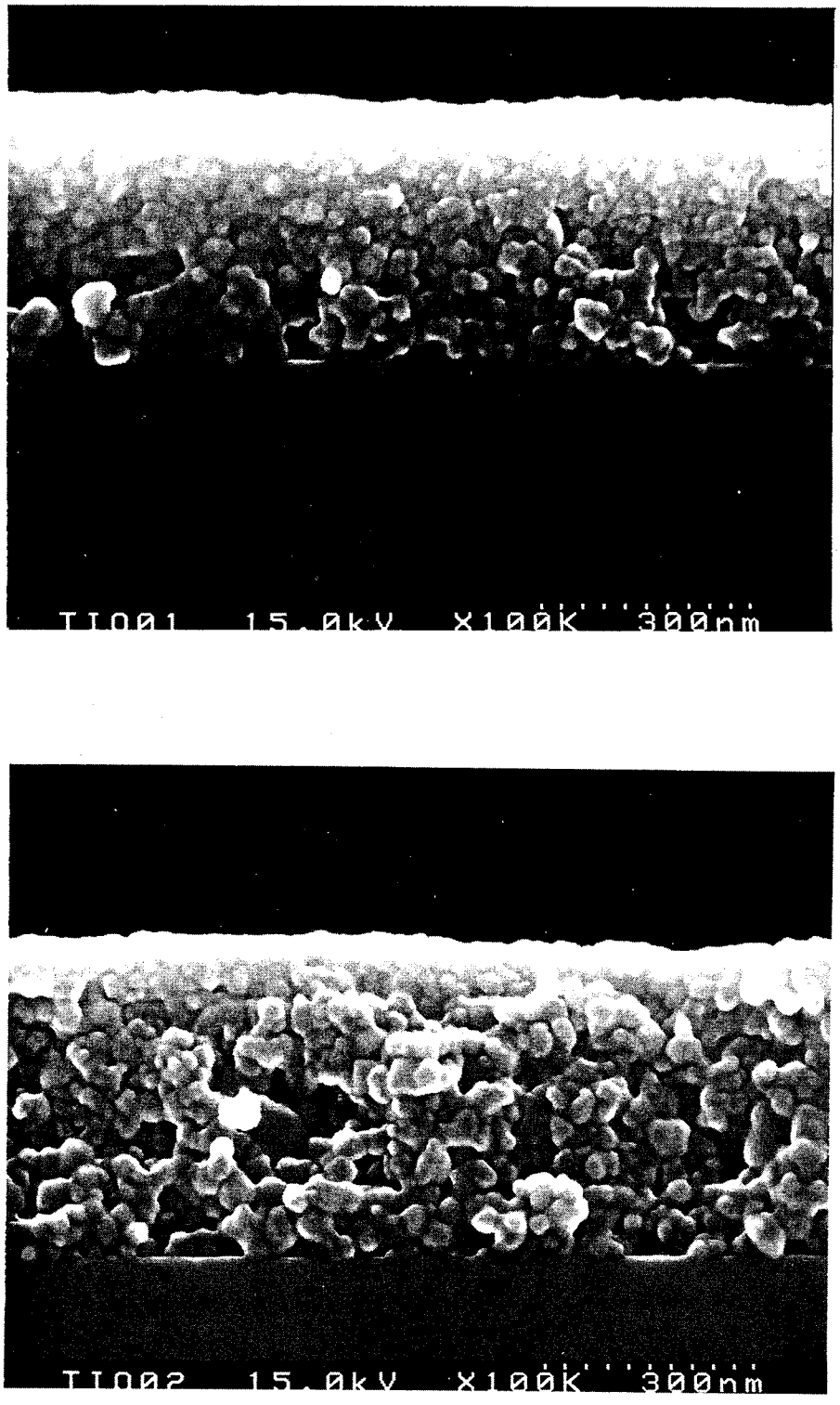

Fig. 3.14 SEM cross-sectional view of a TiO_2 films deposited at a pulling speed of 0.1 mm/s (top) and 0.2 mm/s (bottom) by sol-gel dip-coating method.

has been found to increase rapidly with the pulling speed which is shown in Fig. 3.11. Spherical particles of uniform size and shape, with particle size around 15 nm, distributed homogeneously along the thickness of the film, have been obtained by this method and is shown in the SEM cross-sectional view of the film (Fig. 3.12) which is deposited at a pulling speed of 0.3 mm/s.

Figure 3.13 shows the dependence of cell efficiency and FF on the pulling speed. For the cell with pulling speed of 0.1 mm/s, the cell efficiency is quite low, 0.3% only, though the film thickness is around 400 nm. With the increase in the pulling speed, as the film thickness increases, the cell efficiency also increases and rises over 1% at a pulling speed of 0.5 mm/s. Contrary to the efficiency which increases gradually with pulling speed, FF drops sharply from 0.53 to 0.3 as the pulling speed increases from 0.1 mm/s to 0.2 mm/s after which it increases again. The decrease in FF may be due to the fact that the film deposited at higher pulling speed (0.2 mm/s) is less compact and the particles are in less intimate contact with each other than the film which is deposited at lower pulling speed (0.1 mm/s) resulting in higher film resistance. This statement is justified when we look at the SEM cross-sectional views of the two films which are shown in Fig. 3.14. It can be easily noticed that the top film (pulling speed 0.1 mm/s) is more compact than the bottom one (pulling speed 0.2 mm/s) where voids and pores are much more pronounced than the top one. However, the reason for subsequent increase in FF with pulling speed can not be described by this phenomenon and has yet to understand.

Figure 3.15 shows the transmission spectrum of a complete DNC cell where the TiO_2 film is prepared with a pulling speed of 0.3 mm/s, together with the transmission spectrum of the bare substrate. It shows the cell to be highly transparent, with highest transparency of 65% at 650 nm and near or over 50% almost in the whole visible region which demonstrates its suitability for window application.

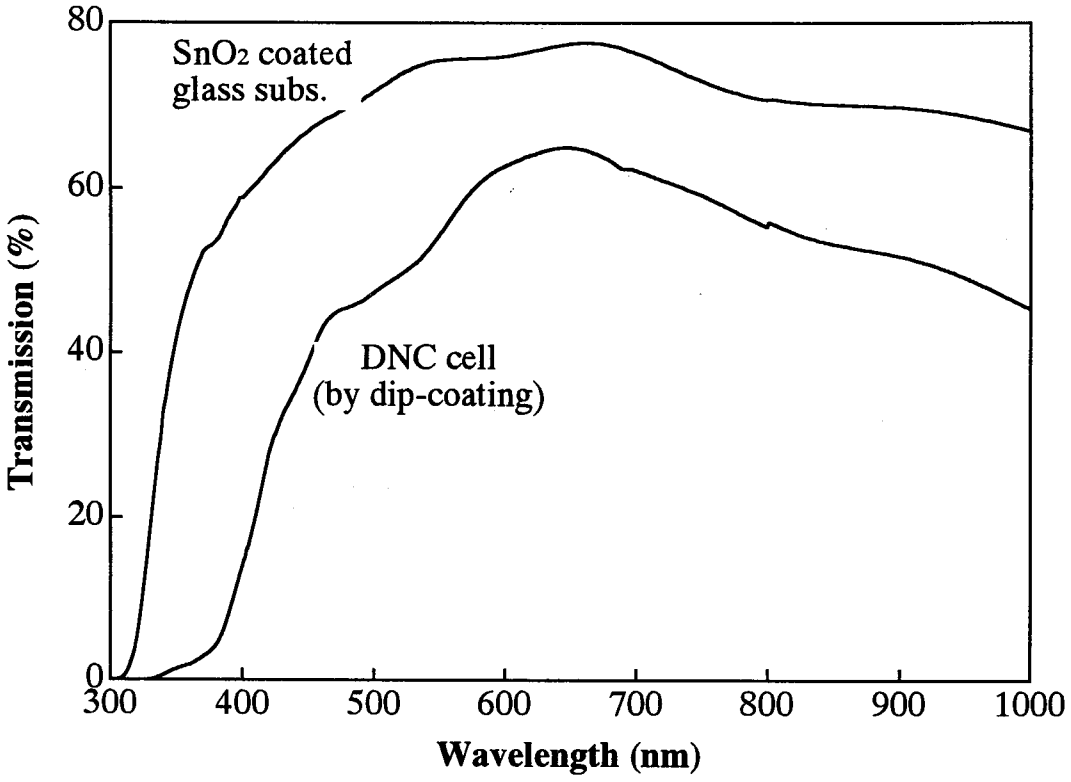

Fig 3.15 Transmission spectrum of a dye-sensitized TiO_2 solar cell with TiO_2 films being prepared by dip-coating method (pulling speed 0.3 mm/s), along with that of the bare SnO_2 coated glass substrate.

3.5 Conclusions

A new type of PEC solar cell developed by Gratzel and his group, namely, dye-sensitized nano-crystalline TiO_2 solar cell, has been discussed and the results on our preliminary investigation of the cell are presented. The cell can be prepared from medium purity materials using low-cost process. Further, the materials used are environmentally benign removing any concern of pollution, whereas Cd (CdTe, CdS) and Se ($CuInSe_2$) based solar cells, which are vied as potential candidate for thin film solar cell, pose serious threat to environmental cleanliness.

The TiO_2 thin films, used to prepare DNC cells, are deposited by spreading of TiO_2 colloidal sol using a glass rod and by sol-gel dip-coating method. In the glass rod spreading method, effect of triton-X addition to the colloidal sol of TiO_2 on the film surface morphology and cell performance has been studied. Slight amount of triton-X addition to the sol has been found to have a profound effect

on the surface morphology and cell performance. Almost five times increase in the short-circuit current has been observed for the cell with triton-X than that of the cell without triton-X. Densely populated large cracks are observed for the TiO_2 films that are prepared using the sol which contains no triton-X. Slight addition (0.25 vol %) of triton-X assists in spreading the sol on the substrate and, thereby, the formation of a smooth surface. However, excess amount of triton-X addition results in reformation of the cracks and degradation of the cell performance. Highest efficiency and FF has been obtained for the cell with 0.5 vol % of triton-X addition. It is concluded that the best performance of a cell can be obtained with maximum amount of triton-X addition for which no crack formation takes place.

In the sol-gel dip-coating method, the effect of pulling speed on the cell performane has been studied. For the cell with pulling speed of 0.1 mm/s, the cell efficiency was quite low, 0.3% only, though the film thickness was around 400 nm. With the increase in the pulling speed, as the film thickness increased, the cell efficiency also increased and rose over 1% at a pulling speed of 0.5 mm/s. One major advantage of this method is this that very thin (few tens of nm to several 100 nm) and highly transparent films of TiO_2 on large substrate can be deposited by this method which can be used to develop transparent or semi-transparent DNC cells suitable for window application. Transmittance of a typical DNC cell prepared using sol-gel derived TiO_2 films showed highly transparent nature of it, with highest transparency of 65% at 650 nm and near or over 50% almost in the whole visible region which demonstrates its suitability for window application.

References

[1] B. O' Regan and M. Gratzel, *Nature* **353** (1991) 737.

[2] M. Gratzel, in *Semiconductor Nanoclusters - Physical, Chemical and Catalytic Aspects*, P.V. Kamat and D. Meisel (eds), Elsevier Science Publishers B. V., Amsterdam, The Netherlands, 1997, pp. 353-461.

[3] A. Fujishima and K. Honda, *Nature* **238** (1972) 37.

[4] H. O. Finklea, in *Semiconductor Electrodes,* H. O. Finklea (ed), Elsevier Science Publishers B. V., Amsterdam, The Netherlands, 1988.

[5] M. D. Archer, *J. Appl. Electrochem.* **5** (1975) 17.

[6] Y. Matsumoto, J. Kurimoto, T. Shimizu and E. Sato, *J. Electrochem. Soc.* **128** (1981) 1040.

[7] J. F. Houlihan, D. B. Armitage, T. Hoovler and D. Bonaquist, *Mater. Res. Bull.* **13** (1978) 1205.

[8] A. Monnier and J. Augustynski, *J. Electrochem. Soc.* **127** (1980) 1576.

[9] Y. Takahashi, A. Ogiso, R. Tomoda, K. Sugiyama, H. Minoura and M. Tsuiki, *J. Chem. Soc. Faraday Trans. I* **78** (1982) 2563.

[10] M. M. Rahman, T. Miki, K. M. Krishna, T. Soga, K. Igarashi, S. Tanemura and M. Umeno, *Mater. Sci. Engg. B* **41** (1996) 67.

[11] K. M.Krishna, M. Sharon and M. K. Mishra, *J. Phys. Chem. Solids* **57** (1996) 615.

[12] J. B. Goodenough, A. Hamnet, M. P. Dare-Edwards, G. Campet and R. D. Wright, *Surf. Sci.* **101** (1980) 531.

[13] M.P.Dare-Edwards, J.B.Goodenough, A. Hamnet, K. R. Seddon and R. D. Wright, *Faraday Disc. Chem. Soc.* **70** (1980) 285.

[14] D. Duonghong, N. Serpone and M. Gratzel, *Helv. Chim. Acta* **67** (1984) 1012

[15] J. DeSilvestro, M. Gratzel and L. Kavan, J. Moser and J. Augustynski, *J. Am. Chem. Soc.* **107** (1985) 2988.

[16] W. West, *Proc. Vogel Centennial Symp., Photogr. Sci. Eng.* **18** (1974) 35.

[17] J. Moser, *Monatsh. Chem.* **8** (1887) 373.

[18] H. Gerischer and H. Tributsch, *Ber. Bunsenges. Phys. Chem.* **72** (1968) 437.

[19] M.K. Nazeeruddin, A. Kay, I. Rodicio, R. Humphry-Baker, E. Muller, P. Liska, N. Vlachopoulos and M. Gratzel, *J. Am. Chem. Soc.* **115** (1993) 6382.

[20] A. Hagfeldt and M. Gratzel, *Chem. Rev.* **95** (1995) 49.

[21] F. Cao, G. Oskam, G. J. Meyer and P. C. Searson, *J. Phys. Chem.* **100** (1996) 17021.

[22] S. E. Lindquist, H. Lindstrom, H. Rensmo, S. Sodergren, A. Solbrand and H. Pettersson, *SPIE* **2255** (1994) 803.

[23] S. Y. Huang, G. Schlichthorl, A. J. Nozik, M. Gratzel and A. J. Frank, *J. Phys. Chem. B* **101** (1997) 2576.

[24] J. Ferber, R. Stangl and J. Lutjer, *Solar Energy Materials and Solar Cells* **53** (1998) 29.

[25] T. A. Heimer, C. A. Bignozzi, G. J. Meyer, *J. Phys. Chem.* **97** (1993) 11987.

[26] M. Gratzel, *AIP Conf. Proc.* 404 (1997) 119.

[27] B. O' Regan, J. Moser, M. Anderson and M. Gratzel, *J. Phys. Chem.* **94** (1990) 8720.

[28] G. Hodes, I. D. J. Howell and L. M. Peter, *J. Electrochem. Soc.* **139** (1992) 3136.

Chapter 4

Prospect of a solid-state solar cell based on TiO_2

4.1 Introduction

Development of dye-sensitized nano-crystalline TiO_2 photoelectrochemical (PEC) solar cell has revealed the inherent potential of TiO_2 as material for solar cell application due to its low cost, simple preparation technique and non-toxicity [1, 2]. However, the low stability suffered by the liquid junction cell demands development of solid-state counterpart of this cell. In this chapter, a solid-state heterojunction solar cell based on TiO_2 is proposed and a theoretical evaluation of the cell performance is made. First, a model for our proposed *n*-TiO_2/*p*-$CuInSe_2$ heterojunction solar cell has been developed and its efficiency has been calculated in order to find out its feasibility as a photovoltaic energy converter. As mentioned in chapter 1, there exist a high spike due to discontinuity at the conduction band edges of TiO_2 and $CuInSe_2$. No theoretical model exists to date for the calculation of heterojunction solar cell efficiency with high ΔE_C ($\Delta E_C > 0.1$ eV), where ΔE_C is the conduction band (CB) discontinuity between the two materials at the interface. Our model is developed using the established theories of current conduction mechanism in Schottky barrier diodes with a varying barrier height as the junction voltage of the cell varies.

Due to the high spike, which hinders the flow of photogenerated electrons from $CuInSe_2$ to TiO_2, the cell efficiency is very low. A new solar cell material $Pb_xTi_{1-x}O_2$ is proposed as a window material of the cell instead of TiO_2 to reduce this high spike. It has been shown by Krishna et al. in a

theoretical work that the band gap of TiO_2 can be varied by mixing it with PbO_2 at different proportions[3]. With the decrease of band gap there is an increase in electron affinity and consequently the difference between electron affinities of the two materials, $Pb_xTi_{1-x}O_2$ and $CuInSe_2$, decreases. A theoretical study of the performance of such a cell (n-$Pb_xTi_{1-x}O_2$/p-$CuInSe_2$) is also made. This solar cell, besides being cheap in cost and easy to fabricate, would be much more stable than the dye-sensitized TiO_2 PEC solar cell because of its solid state nature.

4.2 n-TiO_2/p-$CuInSe_2$ solar cell

4.2.1 Model development

4.2.1.1 Assumptions

Certain assumptions are made in the model developed for the performance study of our proposed n-TiO_2/p-$CuInSe_2$ solar cell.

(1) The device is a true n-p heterojunction with a band diagram under illumination as shown in Fig. 4.1.

(2) Because of wide band gap (3.2 eV) of TiO_2, photocurrent is generated mostly in $CuInSe_2$ film and those in TiO_2 can be neglected.

(3) Because of the high barrier height (ΔE_C=0.48 eV) at the junction, transmission of photogenerated carriers are limited by quantum tunneling probability.

(4) Dark Currents are mainly due to thermionic emission over and tunneling current through the barrier.

(5) Any loss of photogenerated carriers due to recombination is neglected.

(6) There is also no reflection loss in the cell.

4.2.1.2 Computational strategy

The built-in voltage V_b of a heterojunction at thermal equilibrium is given by

$$V_b = \frac{1}{q}\left(\chi_2 - \chi_1 + \frac{E_{g2}}{2} - \frac{E_{g1}}{2} + kT \ln \frac{N_{D1}N_{A2}}{n_{i1}n_{i2}}\right) \quad (1)$$

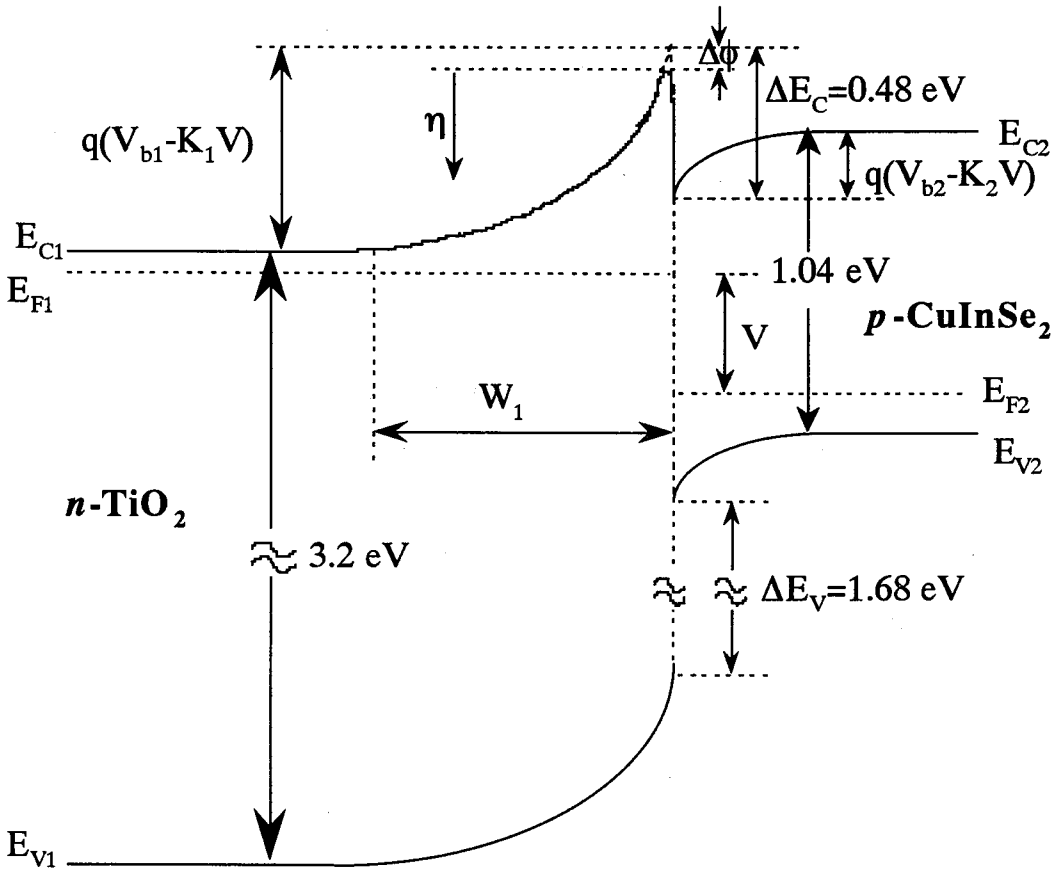

Fig. 4.1 Energy band diagram of n-TiO_2/p-$CuInSe_2$ cell under illumination.

Subscripts 1 and 2 refer to the oxide window and the selenide absorber respectively. Also, χ, E_g, N_D, N_A and n_i are electron affinity, band gap, donor doping density, acceptor doping density and intrinsic carrier density, respectively. q is the magnitude of electronic charge, k is the Boltzmann constant and T is the absolute temperature. n_{i1} and n_{i2} are calculated from

$$n_{i1} = \sqrt{N_{c1}N_{v1}}\exp\left(-E_{g1}/2kT\right) \quad \text{and} \tag{2a}$$

$$n_{i2} = \sqrt{N_{c2}N_{v2}}\exp\left(-E_{g2}/2kT\right) \tag{2b}$$

where N_C and N_V are effective densities of states in the conduction and valence bands, respectively.

The total built-in potential V_b is equal to the sum of the partial built-in voltages ($V_{b1} + V_{b2}$), where V_{b1} and V_{b2} are the electrostatic potentials supported at equilibrium by semiconductors 1 and 2, respectively. Solving Poisson's equation in the depletion region of the junction, gives V_{b1} and V_{b2} as

$$V_{b1} = \frac{qN_{D1}W_{10}^2}{2\varepsilon_{r1}\varepsilon_0} \tag{3a}$$

$$V_{b2} = \frac{qN_{A2}W_{20}^2}{2\varepsilon_{r2}\varepsilon_0} \tag{3b}$$

Here, W_{10} and W_{20} are the thermal equilibrium widths of the space charge regions, ε_r is the low frequency relative permittivity and ε_0 is the permittivity of free space.

In non-equilibrium, the assumption of quasi-equilibrium gives the net voltages $V_{b1} - V_1$ and $V_{b2} - V_2$ as

$$V_{b1} - V_1 = \frac{qN_{D1}W_1^2}{2\varepsilon_{r1}\varepsilon_0} \tag{4a}$$

$$V_{b2} - V_2 = \frac{qN_{A2}W_2^2}{2\varepsilon_{r2}\varepsilon_0} \tag{4b}$$

V_1 and V_2 are the components of the externally applied voltage appearing across the respective junction space charge regions. The non-equilibrium space charge region widths W_1 and W_2 are given by

$$W_1 = \left[\frac{2N_{A2}\varepsilon_{r1}\varepsilon_{r2}\varepsilon_0(V_b - V)}{qN_{D1}(\varepsilon_{r1}N_{D1} + \varepsilon_{r2}N_{A2})}\right]^{\frac{1}{2}} \tag{5a}$$

$$W_2 = \left[\frac{2N_{D1}\varepsilon_{r1}\varepsilon_{r2}\varepsilon_0(V_b - V)}{qN_{A2}(\varepsilon_{r1}N_{D1} + \varepsilon_{r2}N_{A2})}\right]^{\frac{1}{2}} \tag{5b}$$

The dark current of the cell is assumed to be comprised of thermionic emission and tunneling current through the barrier. Thermionic emission current will be mainly due to transport of electrons from TiO_2 to $CuInSe_2$ over the potential barrier of height $q(V_{b1} - K_1V)$ where $K_1 = V_1/V$. Since electrons are minority carriers in $CuInSe_2$, emission of electrons from $CuInSe_2$ to TiO_2 are neglected. This gives thermionic emission current[4]

$$J_{th} = A^*T^2 \exp\left(-\frac{V_{b1}}{V_T}\right)\exp\left(\frac{K_1V}{V_T}\right) \tag{6}$$

Here, A^* is the effective Richardson constant and V_T is the thermal voltage equal to kT/q.

Tunneling component of the dark current will be mainly due to the tunneling of conduction electrons from TiO_2 to $CuInSe_2$. Tunneling of holes from $CuInSe_2$ to TiO_2 can be neglected because of high ΔE_V (1.68 eV). The tunneling current from TiO_2 to $CuInSe_2$ is proportional to the quantum transmission coefficient, P_T, multiplied by the occupation probability in TiO_2 and the unoccupied

probability in $CuInSe_2$ and is given by[4]

$$J_t = \frac{A^* T}{k}\int_0^{\Delta E_C - \Delta\phi} F_1(\eta)P_T(\eta)\{1 - F_2(\eta)\}d\eta \tag{7}$$

Here, $F_1(\eta)$ and $F_2(\eta)$ are the Fermi-Dirac distribution functions for TiO_2 and $CuInSe_2$ respectively. η is measured downward from the potential maximum (Fig. 4.1).

The occupation probability $F_1(\eta)$ in TiO_2 is given by

$$F_1(\eta) = \frac{1}{1 + \exp\{(E - E_{F1})/kT\}} \tag{8}$$

where $E - E_{F1} = qV_{b1} - qK_1V + E_{C1} - E_{F1} - \Delta\phi - \eta$.

E, E_{F1} and E_{C1} have their usual meaning and $\Delta\phi$ is the barrier height lowering due to Schottky effect and is given by

$$\Delta\phi = \frac{q}{2\varepsilon_{r1}\varepsilon_0}\left(\frac{N_{D1}W_1}{\pi}\right)^{\frac{1}{2}} \tag{9}$$

$1 - F_2(\eta)$ is the unoccupied probability of states in $CuInSe_2$ and as can be seen from Fig. 4.1, no state is available in $CuInSe_2$ for an electron to occupy when $\eta > \Delta E_C - \Delta\phi$. So we approximate $1 - F_2(\eta)$ as

$$\begin{aligned} 1 - F_2(\eta) &\approx 1 \text{ , for } 0 < \eta < \Delta E_C - \Delta\phi \\ &= 0 \text{ , for } \eta > \Delta E_C - \Delta\phi \end{aligned} \tag{10}$$

Transmission probability P_T is derived as (see Appendix A)

$$P_T = \left[\exp\left\{\frac{2\pi}{h}\frac{(2m^*)^{\frac{1}{2}}W_1E_{rel}}{\sqrt{q(V_{b1} - K_1V)}}\left(\frac{1}{2}\sinh 2u - u\right)\right\} + \frac{1}{4}\exp\left\{-\frac{2\pi}{h}\frac{(2m^*)^{\frac{1}{2}}W_1E_{rel}}{\sqrt{q(V_{b1} - K_1V)}}\left(\frac{1}{2}\sinh 2u - u\right)\right\}\right]^{-2} \tag{11}$$

Here, h is Planck constant, m^* is the effective mass of tunneling electron and

$$u = \cosh^{-1}\left(\sqrt{\frac{q(V_{b1} - K_1V)}{E_{rel}}}\right)$$

E_{rel} is the energy of an electron and is measured relative to the bottom of the conduction band of TiO_2

in the bulk and is given by

$$E_{rel}=q(V_{b1}-K_1V)-\Delta\phi-\eta. \tag{12}$$

Now the photocurrent is assumed to be due to absorption of photons in $CuInSe_2$ and that in TiO_2 is neglected due to its high band gap. This photocurrent is given by the photocurrent I_L, that would have flown if there were no barrier at the junction, multiplied by the quantum transmission probability $P_T(V)$ of photogenerated electrons, that is,

$$J_{ph}=P_T(V)I_L \tag{13}$$

Transmission probability $P_T(V)$ for photogenerated electrons in $CuInSe_2$ is the same as that given by eqn. (11) except that here E_{rel} instead of being continuously varying energy from $(qV_{b1}-qK_1V-\Delta\phi)$ to $(qV_{b1}-qK_1V-\Delta E_C)$, it is given by $(qV_{b1}-qK_1V-\Delta E_C)$ plus the average thermal energy, E_{th} , of photogenerated electrons in $CuInSe_2$ which is equal to $3kT/2$, i.e.,

$$E_{rel}=q(V_{b1}-K_1V)-\Delta E_C+E_{th} \tag{14}$$

Combining equations (6), (7) and (13), we get the complete $I-V$ characteristics of the cell under illuminaation and is given by

$$J=A^*T^2\exp\left(-\frac{V_{b1}}{V_T}\right)\exp\left(\frac{K_1V}{V_T}\right)+\frac{A^*T}{k}\int_0^{\Delta E_C-\Delta\phi}F_1(\eta)P_T(\eta)\{1-F_2(\eta)\}d\eta-P_T(V)I_L \tag{15}$$

The sum of the first two terms of eqn. (15) is the forward diode current density in the dark and the loss current density under illumination. However, no effect of series or shunt resistance or recombination losses are taken into account.

4.2.2 Results and discussion

The I-V characteristics of n-TiO_2/p-$CuInSe_2$ in ideal case, i.e., not considering the recombination losses, is evaluated according to eqn. (15) considering an illumination of 1 SUN at AM 1.5 condition and is shown in Fig. 4.2. Most of the parameter values, used in the calculation, are taken from literature[5, 6] and are summerized in table 4.1. High values of N_{D1} (10^{20} cm^{-3}) and N_{A2} (2.5×10^{21} cm^{-3}) were chosen in order to keep the barrier width small, thereby increase the tunneling

TABLE 4.1 : General parameter values

$TiO_2/Pb_xTi_{1-x}O_2$		$CuInSe_2$	
Parameter	Value	Parameter	Value
N_{c1} (cm^{-3})*	4.12×10^{21}	N_{c2} (cm^{-3})	5×10^{18}
N_{v1} (cm^{-3})*	4.12×10^{21}	N_{v2} (cm^{-3})	10^{19}
χ_1 (eV)	4 (TiO_2)	χ_2 (eV)	4.48
	4.48 ($Pb_xTi_{1-x}O_2$)	ε_{r2} $(-)$	13.6
ε_{r1} $(-)$	48	E_{g2} (eV)	1.04
E_{g1} (eV)	3.2 (TiO_2)	μ_{n2} $(cm^2V^{-1}s^{-1})$	150
	2.58 ($Pb_xTi_{1-x}O_2$)	τ_{n2} (s)	10^{-10}
$\mu_{p1}(cm^2V^{-1}s^{-1})$	0.1	L_{n2} (cm)	$1.97\text{x}10^{-5}$
τ_{p1} (s)	3.5×10^{-11}	τ_{02} (s)	40×10^{-9}
L_{p1} (cm)	3×10^{-7}		
m^*	$30m_e$		

*Data not available. N_{c1} and N_{v1} are assumed to be equal and have been calculated assuming an effective electron mass of $30m_e$[6]. m_e is the electron rest mass.

probability. N_{A2} is chosen to be higher than N_{D1}. This makes depletion width W_2 smaller than the depletion width W_1, as a result, greater part of the built-in voltage V_b is supported by TiO_2, which means $V_{b1} > V_{b2}$. This keeps the bottom level of CB (E_{C1}) of TiO_2 lower than that of $CuInSe_2$ and makes the tunneling of photogenerated electrons from $CuInSe_2$ to TiO_2 possible. An open circuit voltage $V_{OC} = 0.68$ V, short circuit current $I_{SC} = 4.27$ mA/cm^2, fill factor $= 0.44$ and efficiency $\eta =$ 1.51% have been obtained.

Transport of photogenerated carriers in $CuInSe_2$ film is limited by the quantum tunneling probability of the carriers through the high barrier at the conduction band edge of $TiO_2/CuInSe_2$ interface. The electron affinities of TiO_2 and $CuInSe_2$ are 4 eV and 4.48 eV respectively which give a conduction band discontinuity of 0.48 eV [7]. Even after taking into account the barrier height lowering due to Schottky effect, which is found to be around 0.08 eV, the barrier height is (0.48 −0.08=) 0.4 eV which is still too high and limits the quantum tunneling probability to only 15%. Fill factor of this cell is also low. As the junction voltage increases, the photocurrent decreases.

To explain this phenomenon, we have taken W_B as the width of the barrier at an energy

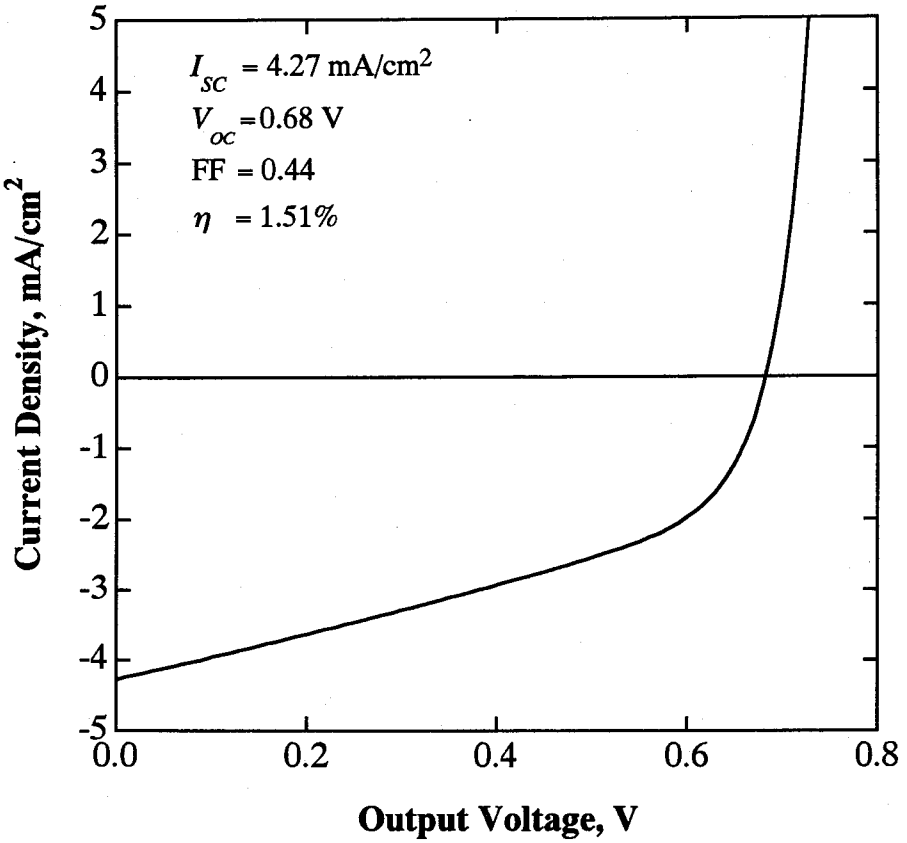

Fig. 4.2. $I-V$ characteristics of n-TiO_2/p-$CuInSe_2$ solar cell at 1 SUN AM 1.5 condition.

level where the tunneling of photogenerated electrons takes place. We call W_B as the effective barrier width and is derived as(see Appendix B)

$$W_B = W_1\left\{1-\sqrt{\frac{q(V_{b1}-K_1V)-\Delta E_C+E_{th}}{q(V_{b1}-K_1V)}}\right\} \tag{16}$$

The variation of W_B and transmission probability $P_T(V)$ with junction voltage V is shown in Fig. 4.3. It is seen that as the junction voltage V increases, effective barrier width W_B increases and transmission probability $P_T(V)$ decreases. This in turn decreases the photocurrent and leads to a low fill factor. One might be tempted to increase the tunneling probability by increasing the doping density of TiO_2 film and thereby decreasing the depletion width. But in our model a donor doping density $N_{D1}=10^{20}$ cm^{-3} has been assumed which is already too high to be achieved practically.

4.3 n-$Pb_xTi_{1-x}O_2$/p-$CuInSe_2$ solar cell : a modification of n-TiO_2/p-$CuInSe_2$ heterostrucure

Because of the high barrier at the junction of TiO_2/$CuInSe_2$ cell, the cell efficiency is very

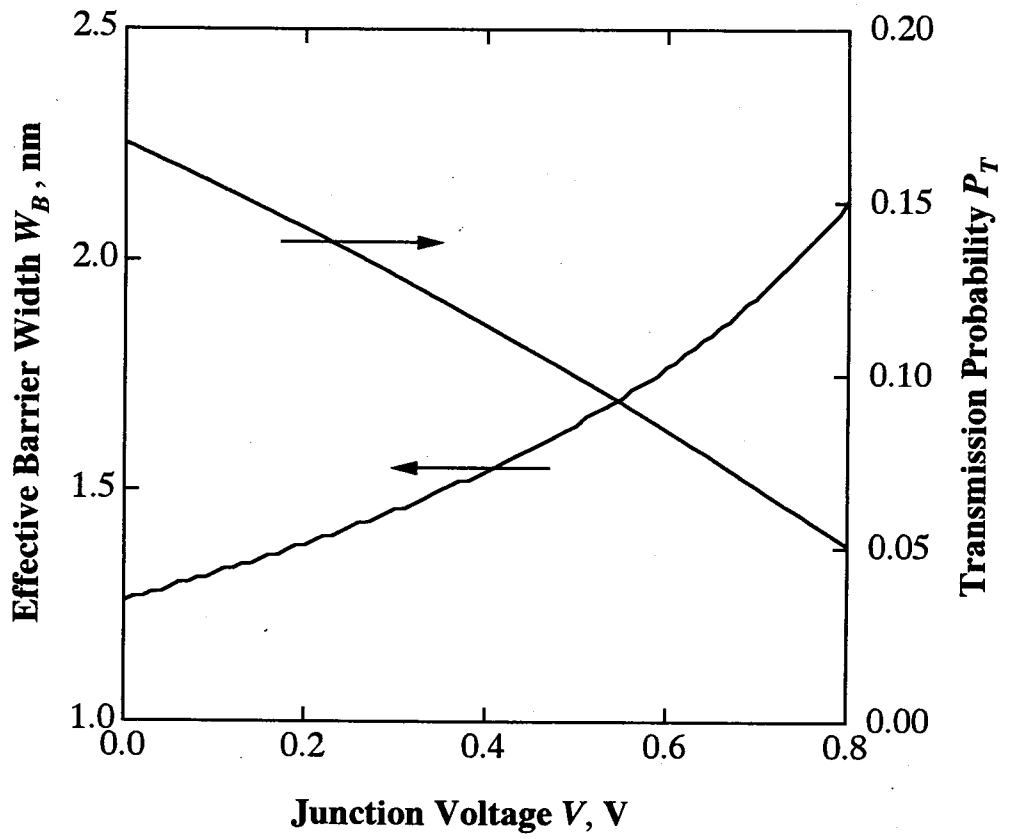

Fig. 4.3 Variation of effective barrier width W_B and transmission probability P_T as a function of junction voltage V for n-TiO_2/p-$CuInSe_2$ solar cell.

low. So in order to reduce or eliminate this barrier, we propose $Pb_xTi_{1-x}O_2$ as the window material instead of TiO_2, where both the band gap and electron affinity of $Pb_xTi_{1-x}O_2$ can be varied by varying x. With the decrease of band gap there is an increase in electron affinity and consequently the difference between the electron affinities of the two materials, $Pb_xTi_{1-x}O_2$ and $CuInSe_2$, decreases. In our calculation, it is assumed that the electron affinities of the two semiconductors perfectly match and that the band gap of $Pb_xTi_{1-x}O_2$ is 2.58 eV. The assumption of these values closely matches with the calculated results of Krishna *et al.*[3] when PbO_2 and TiO_2 are mixed at a ratio of 1:3.

4.3.1 Model development

4.3.1.1 Assumptions

The model is based on the following assumptions:

(1) The device is a true *n-p* heterojunction with a thermal equilibrium band diagram as

shown in Fig. 4.4.

(2) The forward currents both in the dark and under illumination are comprised of three components: minority carrier diffusion current in p-$CuInSe_2$, recombination current

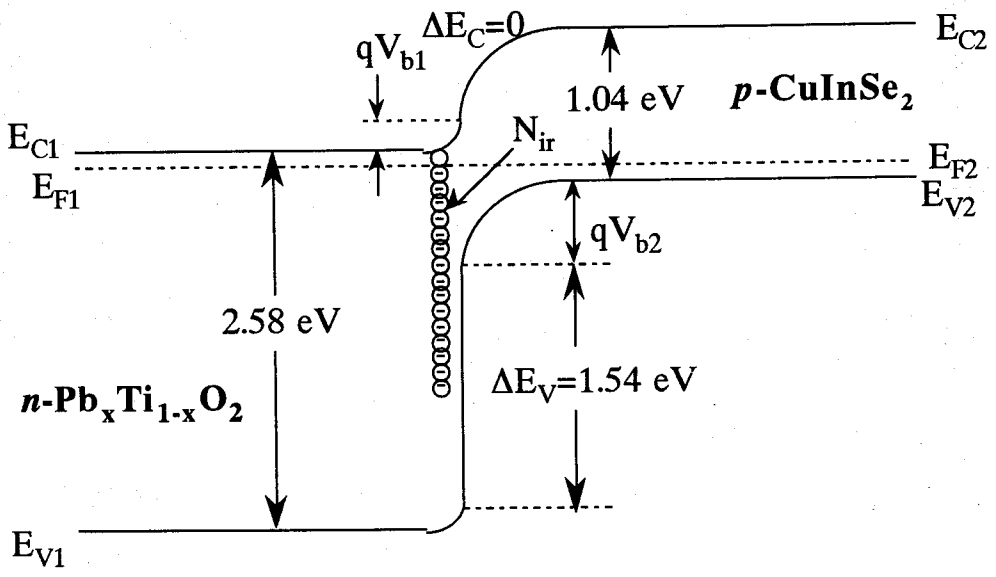

Fig. 4.4 Energy band diagram of n-$Pb_xTi_{1-x}O_2$/p-$CuInSe_2$ heterojunction at thermal equilibrium.

at the hetero-interface and recombination current in the space charge region.

(3) Interface recombination centers are acceptor-like and the rate of recombination is limited by the availability of holes. That means of the electron and the hole trapped alternately to complete a recombination event, the electron spends considerably more time while in trap than does a hole. As a result, the recombination center is negatively charged most of the time. For simplicity, it is assumed that the interface recombination centers are negatively charged, giving rise to an interface charge density $-qN_{ir}$ ($C\,cm^{-2}$) where N_{ir} (cm^{-2}) is the interface recombination level density [8].

(4) Electron affinities of both $Pb_xTi_{1-x}O_2$ (χ_1) and $CuInSe_2$ (χ_2) are equal to 4.48 eV.

4.3.1.2 Computational strategy

The interface-recombination current density is given by [8],

$$J_{ir}(V) = qS_{ip}\Delta p_i(V) = q\sigma_{ip}v_{th}N_{ir}\Delta p_i(V) \tag{17}$$

where $S_{ip} = \sigma_{ip}v_{th}N_{ir}$ is the hole recombination velocity at the interface. σ_{ip} is the hole capture cross-section, v_{th} is its thermal velocity and $\Delta p_i(V)$ is the excess hole concentration at the interface and is given by

$$\Delta p_i(V) = N_{A2}\exp\left(-\frac{V_{b2}}{V_T}\right)\left\{\exp\left(\frac{K_2V}{V_T}\right)-1\right\} \tag{18}$$

Here, V_{b2} and V have the same meaning as explained before and $K_2 = V_2/V$, where V_2 can be calculated using eqn. (4b) except that W_2 is represented by the following equation which has been derived solving Poisson's equation in the depletion region considering the presence of interface charge density $-qN_{ir}$.

$$W_2 = \frac{-b+\sqrt{b^2-4ac}}{2a} \tag{19}$$

where

$$a = \frac{qN_{A2}}{2\varepsilon_{r2}\varepsilon_0}\left(1+\frac{N_{A2}\varepsilon_{r2}}{N_{D1}\varepsilon_{r1}}\right) \tag{20a}$$

$$b = \frac{qN_{A2}N_{ir}}{\varepsilon_{r1}\varepsilon_0 N_{D1}} \quad \text{and} \tag{20b}$$

$$c = \frac{qN_{ir}^{\ 2}}{2\varepsilon_{r1}\varepsilon_0 N_{D1}} - (V_b - V) \tag{20c}$$

Combining equations (17) and (18), the interface recombination current density

$$J_{ir} = J_{0ir}\left\{\exp\left(\frac{K_2V}{V_T}\right)-1\right\} \tag{21}$$

where

$$J_{0ir} = q\sigma_{ip}v_{th}N_{ir}N_{A2}\exp\left(-\frac{V_{b2}}{V_T}\right) \tag{22}$$

The space charge recombination current is proportional to the intrinsic carrier concentration n_i, and in $Pb_xTi_{1-x}O_2$, it is negligible because of its wide band gap. So, we can assume that the space charge recombination current occurs entirely in $CuInSe_2$[9]. Now the standard equations for the space charge recombination and the diffusion currents in $CuInSe_2$ are given by

$$J_{scr} = J_{0sc}\left\{\exp\left(\frac{K_2 V}{V_T}\right) - 1\right\} \tag{23}$$

with $$J_{0sc} = \frac{qn_{i2}W_2}{2\tau_{02}} \qquad \text{and} \tag{24}$$

$$J_d = J_{0d}\left\{\exp\left(\frac{V}{V_T}\right) - 1\right\} \tag{25}$$

with $$J_{0d} = \frac{qD_{n2}}{L_{n2}} \cdot \frac{n_{i2}^2}{N_{A2}} \cdot \frac{\frac{D_{n2}}{S_n L_{n2}}\sinh\frac{W_p}{L_{n2}} + \cosh\frac{W_p}{L_{n2}}}{\frac{D_{n2}}{S_n L_{n2}}\cosh\frac{W_p}{L_{n2}} + \sinh\frac{W_p}{L_{n2}}} \tag{26}$$

Here, n_{i2} is the intrinsic carrier concentration and τ_{02} is the effective recombination life time in $CuInSe_2$ space charge region. D_{n2} and L_{n2} are the diffusion co-efficient and the diffusion length in $CuInSe_2$. S_n is the back surface recombination velocity of electrons and W_p is the base width.

The complete *I-V* characteristics of the cell under illumination, without taking into account the effects of series and shunt resistances, is given by

$$J = J_{0ir}\left\{\exp\left(\frac{K_2 V}{V_T}\right) - 1\right\} + J_{0scr}\left\{\exp\left(\frac{K_2 V}{V_T}\right) - 1\right\} + J_{0d}\left\{\exp\left(\frac{V}{V_T}\right) - 1\right\} - J_{ph} \tag{27}$$

The sum of the first three terms of eqn. (27) is the forward diode current density in the dark and the loss current density under illumination. J_{ph} is the photogenerated current density which might be somewhat dependent on the junction voltage through the voltage dependence of the space charge region width. But in our calculation, this dependence is neglected. The complete equation for J_{ph} can be obtained from Ref. 10.

4.3.2 Results and discussion

The same parameter values, that were used for $TiO_2/CuInSe_2$ cell (see Table 1), are also used for $Pb_xTi_{1-x}O_2/CuInSe_2$ cell except the band gap and electron affinity of $Pb_xTi_{1-x}O_2$ which are assumed to be 2.58 and 4.48 eV, respectively. Dependence of open circuit voltage V_{OC} on base doping density N_{A2} and interface recombination level density N_{ir} are investigated first to find out an optimum value of N_{A2}. Then spectral responses in different regions of the cell are evaluated which shows little

dependence of the cell performance on emitter doping density N_{D1}. I-V curve of the cell is drawn with the optimized value of N_{A2}. In case the electron affinities of $Pb_xTi_{1-x}O_2$ and $CuInSe_2$ do not match, ΔE_C will not be zero and there will be an increase or decrease in V_{OC}. The effect of non-zero ΔE_C on V_{OC} of such a cell is also evaluated. Effect of cell thickness, namely base thickness, on photocurrent is investigated and is found that photocurrent increases with increasing base thickness upto a certain value (not shown here) and becomes almost constant when the thickness is increased beyond 2 μm. A base thickness of 2 μm for the main absorber ($CuInSe_2$) is assumed which maximizes the photocurrent of the cell. An window layer ($Pb_xTi_{1-x}O_2$) thickness of 0.5 μm is assumed. Window layer thickness will have little effect on the cell performance unless the effect of series resistance is taken into account. However, a small window layer thickness is always desirable. All the calculations are carried out considering an illumination of 1 SUN at AM 1.5 condition.

4.3.2.1 Open circuit voltage V_{OC}

Figure 4.5 shows the variation of open circuit voltage V_{OC} with base doping density N_{A2} and interface recombination level density N_{ir} . With the increase in base doping density N_{A2}, diffusion current decreases (eqn. 25). This would lead to an increase in V_{OC}. But the increase in N_{A2} also increases interface recombination current J_{ir} (eqn. 21). So, after a certain value of N_{A2}, increase in J_{ir} exceeds decrease in J_d and the total dark current starts increasing which leads to a decrease in V_{OC}. There is a sharp decrease in V_{OC} as interface recombination level density N_{ir} increases from 10^{11} cm^{-2} to 10^{12} cm^{-2}. However, there is a saturation in V_{OC} as N_{ir} is decreased below 10^{11} cm^{-2} and 10^{11} cm^{-2} can be taken as an acceptable value for N_{ir} for the cell to be operated without significant loss. With N_{ir} equal to 10^{11} cm^{-2}, $N_{A2}=5\times10^{15}$ cm^{-3} is found to be the optimum value for maximum V_{OC}.

4.3.2.2 Spectral response

The calculated spectral response curves are shown in Fig. 4.6. Details of the calculation procedure is same as those given in Ref. 10. The spectral response from the window region is shown on a much exaggerated scale. This shows that the spectral response from the window region is very

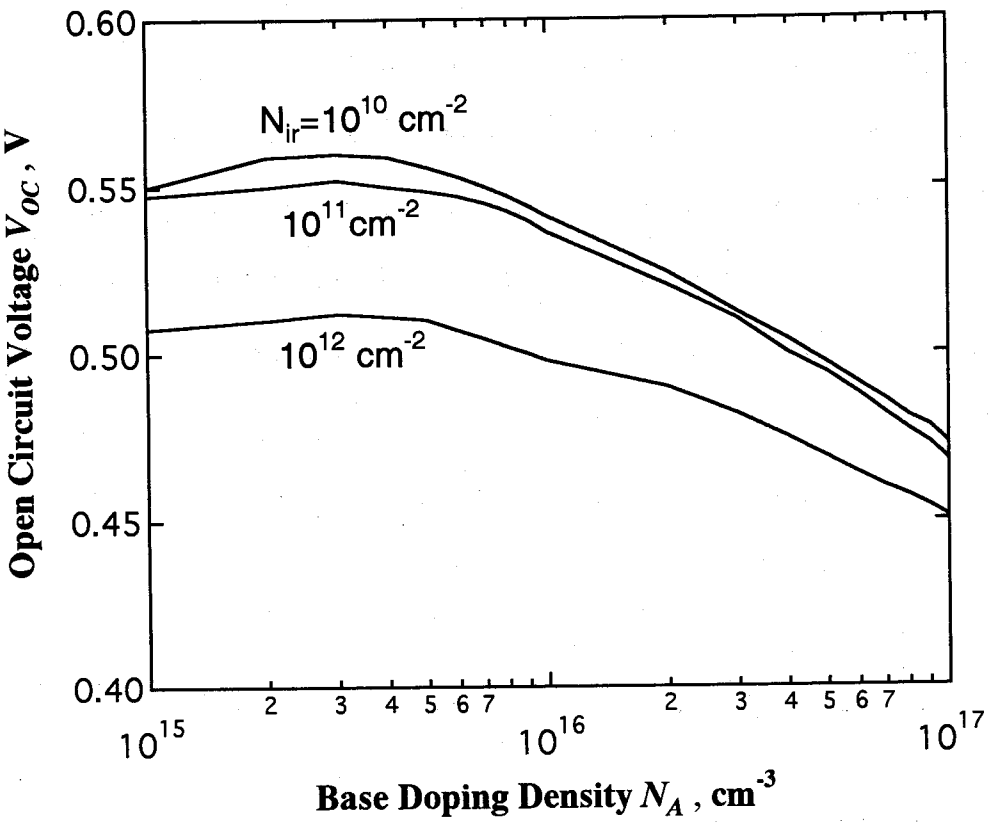

Fig. 4.5 Calculated open circuit voltage V_{OC} of n-$Pb_xTi_{1-x}O_2$/p-$CuInSe_2$ solar cell as a function of base doping density N_A and interface recombination level density N_{ir}.

small and has negligibly small effect on the total spectral response. This is because both the minority carrier diffusion length L_{p1} and mobility μ_{p1} (0.1 cm^2/V.s) in the $Pb_xTi_{1-x}O_2$ film are very small. For this reason, the various parameters of $Pb_xTi_{1-x}O_2$ film, such as thickness and doping density, will have little effect on the cell performance. It is also seen from the figure that the depletion region component of the total spectral response is largest. This is attributed to the fact that because of low doping of $CuInSe_2$, depletion region is extended mainly in $CuInSe_2$ and because of its extremely high absorption coefficient, most of the photons are absorbed in this depletion region.

4.3.2.3 I–V characteristics

The calculated I–V characteristics of our proposed n-$Pb_xTi_{1-x}O_2$/p-$CuInSe_2$, evaluated with the optimum value of N_{A2} (5×10^{15} cm^{-3}), are shown in Fig. 4.7. An emitter doping density $N_{D1}=10^{18}$ cm^{-3} is assumed. An open circuit voltage $V_{OC}=0.54$ V, short circuit current $I_{SC}=36$ mA/cm^2,

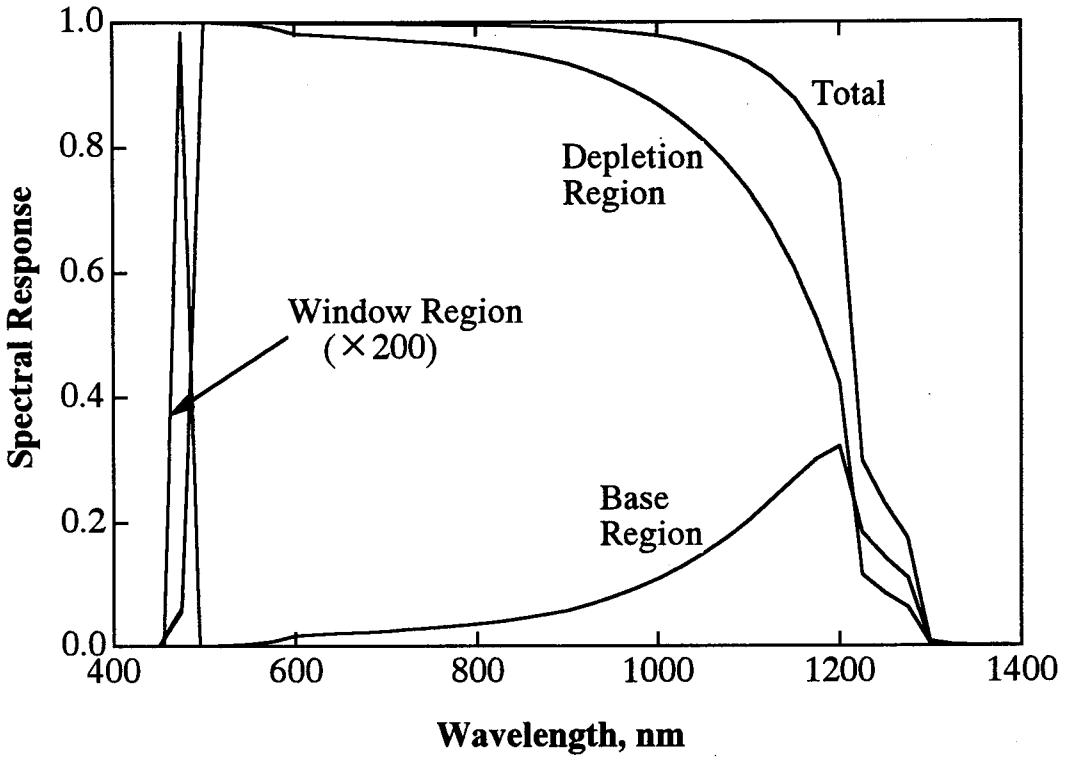

Fig. 4.6 External Spectral response of proposed solar cell under 1 SUN AM 1.5 condition. ($N_D=10^{18}$ cm^{-3}, $N_A=10^{16}$ cm^{-3}, $W_n=0.5$ μm, $W_p=2$ μm, $L_p=3\times10^{-7}$ cm, $\mu_p=0.1$ cm^2/V.s, $S_p=10^6$ cm^2/s, $L_n=1.97\times10^{-5}$ cm, $\mu_n=150$ cm^2/V.s, $S_n=10^6$ cm^2/s)

fill factor = 0.937 and efficiency η = 18.78 % have been obtained. This efficiency (18.78 %) has been obtained without considering the effects of series and shunt resistances and also the recombination in the bulk of $CuInSe_2$. A decrease in the efficiency, as well as in the fill factor, is obvious when these effects will be taken into account. Practical cells are always incorporated with some resistances which cause the cell efficiency and fill factor go down. In our calculation, though efficiency is not that high, fill factor is very high (0.937) which, we believe, is due to omission of these effects, resistivity and bulk recombination.

4.3.2.4 Effect of non-zero ΔE_C

Until now, all the calculations have been done assuming conduction band edge discontinuity $\Delta E_C=\chi_1-\chi_2$ at the heterojunction interface to be equal to zero. However, in reality, there might be some mismatch between electron affinities, χ_1 and χ_2, causing ΔE_C to deviate from zero. Figure 4.8 shows the variation of open circuit voltage V_{OC} as a function of ΔE_C for different values of N_{ir}. It was

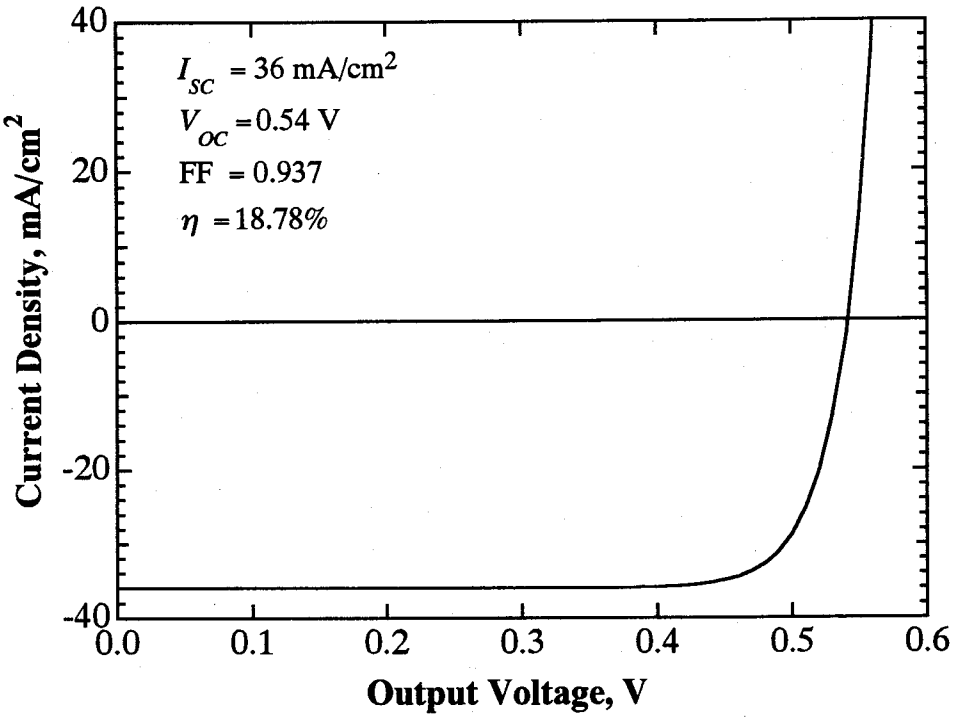

Fig. 4.7 *I-V* characteristics of *n*-$Pb_xTi_{1-x}O_2$/*p*-$CuInSe_2$ solar cell at 1 SUN AM 1.5 condition, assuming ΔE_C=0.

assumed that there will be no hindrance to the flow of photogenerated electrons from $CuInSe_2$ to $Pb_xTi_{1-x}O_2$ for a spike discontinuity of upto 0.1 eV. From Fig. 4.8, it can be seen that for low value of N_{ir}, V_{OC} is almost constant and slightly decreasing for positive ΔE_C. This is because at low value of N_{ir}, dark current is mainly determined by the diffusion current which is nearly independent of ΔE_C. At high value of N_{ir}, V_{OC} decreases as ΔE_C becomes more positive. In this case, dark current is mainly determined by the recombination current because of high value of N_{ir}. As ΔE_C becomes more positive, built-in voltage V_b and consequently V_{b2} decreases. This decrease in V_{b2} increases recombination current J_{ir} (eqn. 21) and decreases open circuit voltage V_{OC}.

4.4 Conclusions

Theoretical performance study of a novel solid state heterojunction solar cell based on low cost material TiO_2 (*n*-TiO_2/*p*-$CuInSe_2$) has been made. A theoretical efficiency of only 1.51% has been obtained under ideal conditions. The high barrier height at the conduction band edge of

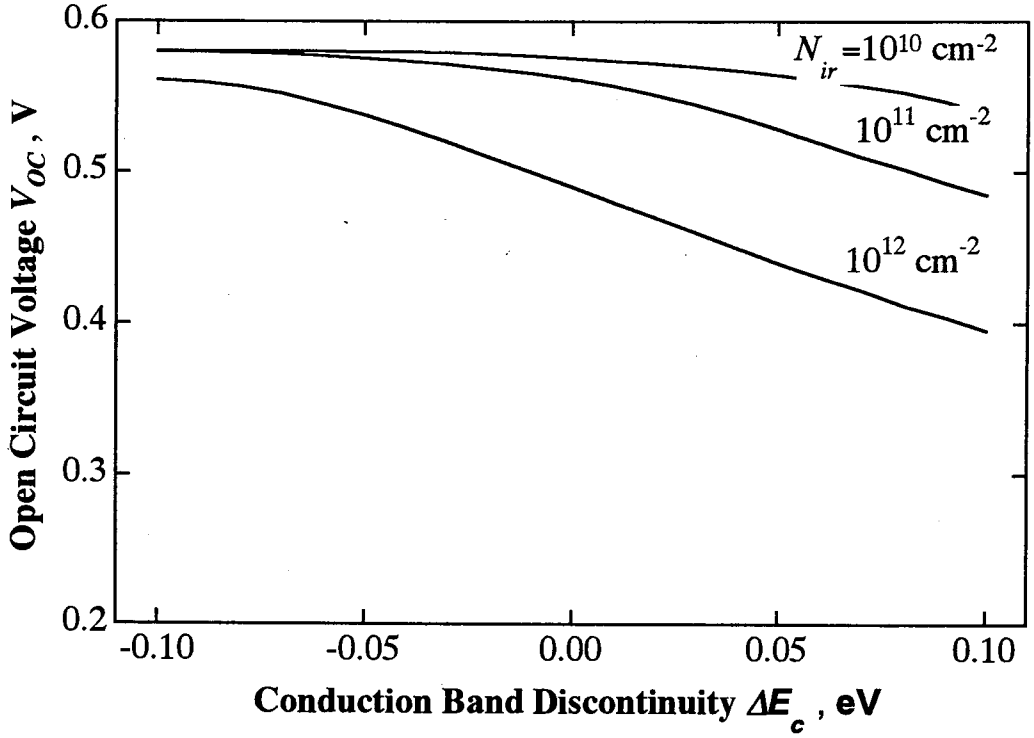

Fig. 4.8 Calculated open circuit voltage V_{OC} as a function of conduction band discontinuity ΔE_C and interface recombination level density N_{ir} for *n*-$Pb_xTi_{1-x}O_2$/*p*-$CuInSe_2$ solar cell.

TiO_2/$CuInSe_2$ interface limits the quantum transmission probability of photogenerated electrons from $CuInSe_2$ to TiO_2 to only 15%. This further decreases with increase in the junction voltage. To reduce the high barrier at the junction, the ternary oxide semiconductor $Pb_xTi_{1-x}O_2$ has been proposed as the top material of the cell instead of TiO_2. Assuming $\Delta E_C = 0$, and no energy loss due to resistance and bulk recombination, efficiency of *n*-$Pb_xTi_{1-x}O_2$/*p*-$CuInSe_2$ solar cell has been calculated and an efficiency of around 18.78% has been obtained at 1 SUN AM 1.5 condition. The efficiency can be further increased by making some optimization with respect to the carrier doping densities and cell thickness. Though $CuInSe_2$ is the main absorber material in the cell, use of oxide semiconductor as a window material makes the cell interesting from a theoretical point of view and simple preparation techniques, such as, sol-gel method for $Pb_xTi_{1-x}O_2$ thin film preparation and electrochemical deposition process for $CuInSe_2$ film growth would certainly keep the cost of the cell to a low value. The results of our preliminary attempt to prepare the top material, $Pb_xTi_{1-x}O_2$, will be discussed in the following chapter.

Appendix A:

Derivation of quantum-mechanical transmission probability P_T

An enlarged view of the conduction-band diagram in the depletion region of TiO_2 is shown in Fig. 4.9 for ease of understanding. It is assumed that the barrier is parabolic so that it can be described by the equation $y=ax^2$ where a is a constant of proportionality. The energy of an electron is measured relative to the bottom of the conduction band of TiO_2 in the bulk and is designated as E_{rel}.

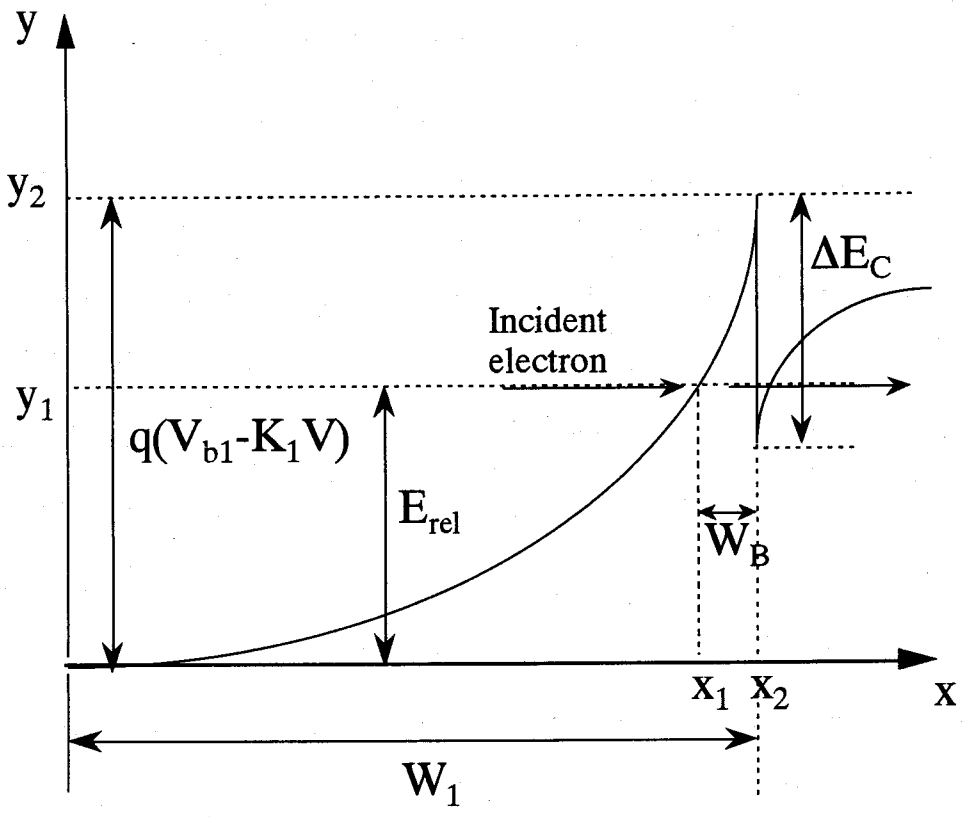

Fig. 4.9 Conduction band diagram in the depletion region of TiO_2.

An electron, with energy E_{rel}, is incident at a point x_1 on the barrier and is transmitted at x_2 (Fig. 4.9). The probability of quantum transmission for this particle, using the Wentzel-Kramers-Brillouin (WKB) approximation, is given by [11]

$$P_T = \left[\exp\left(\frac{1}{\hbar}\int_{x_l}^{x_r} dx\left|p(x)\right|\right) + \frac{1}{4}\exp\left(-\frac{1}{\hbar}\int_{x_l}^{x_r} dx\left|p(x)\right|\right)\right]^{-2} \tag{A.1}$$

where

$$p(x) = \sqrt{2m^*\left(E_{rel} - V(x)\right)} \quad \text{and} \tag{A.2}$$

$$V(x) = y = ax^2 \tag{A.3}$$

Hence, $$p(x) = \sqrt{2m^*\left(E_{rel} - ax^2\right)} \tag{A.4}$$

From Fig. 4.9, at $x = x_2 = W_1$, and $y = y_2 = q(V_{b1} - K_1 V)$. Hence, from eqn. (A.3),

$$a = q(V_{b1} - K_1 V)/W_1^2.$$

Substituting this into eqns. (A.3) and (A.4), we get

$$y = \{q(V_{b1} - K_1 V)/W_1^2\}x^2 \quad \text{and} \tag{A.5}$$

$$p(x) = \sqrt{2m^*\left(E_{rel} - \frac{q(V_{b1} - K_1 V)}{W_1^2}x^2\right)} \tag{A.6}$$

Now we will first evaluate the integral $\int_{x_1}^{x_r} dx|p(x)|$ of eqn. (A.1).

$$\int_{x_1}^{x_r} dx|p(x)| = (2m^*)^{\frac{1}{2}} \int_{x_1}^{x_2} \left(\frac{q(V_{b1} - K_1 V)}{W_1^2}x^2 - E_{rel}\right)^{\frac{1}{2}} dx \tag{A.7}$$

Upon substituting $x = W_1\sqrt{\dfrac{E_{rel}}{q(V_{b1} - K_1 V)}}\cosh u$ in eqn. (A.7), we get

$$\int_{x_1}^{x_r} dx|p(x)| = (2m^*)^{\frac{1}{2}} \frac{W_1 E_{rel}}{\sqrt{q(V_{b1} - K_1 V)}} \int_{x=x_1}^{x=x_2} \sinh^2 u\, du$$

$$= (2m^*)^{\frac{1}{2}} \frac{W_1 E_{rel}}{\sqrt{q(V_{b1} - K_1 V)}} \left[\frac{1}{2}\sinh 2u - u\right]_{x=x_1}^{x=x_2} \tag{A.8}$$

At $x = x_1$, $y = E_{rel}$, and from eqn. (A.5),

$$x_1 = W_1\sqrt{\frac{E_{rel}}{q(V_{b1} - K_1 V)}} \tag{A.9}$$

Hence, $$u_1 = \cosh^{-1}\frac{x_1}{W_1}\sqrt{\frac{q(V_{b1} - K_1 V)}{E_{rel}}} = \cosh^{-1} 1 = 0 \tag{A.10}$$

At $x = x_2$, $$u_2 = \cosh^{-1}\frac{x_2}{W_1}\sqrt{\frac{q(V_{b1} - K_1 V)}{E_{rel}}} = \cosh^{-1}\sqrt{\frac{q(V_{b1} - K_1 V)}{E_{rel}}} \tag{A.11}$$

since $x_2 = W_1$.

From eqns. (A.8), (A.10) and (A.11) we get

$$\int_{x_1}^{x_r} dx|p(x)| = (2m^*)^{\frac{1}{2}} \frac{W_1 E_{rel}}{\sqrt{q(V_{b1} - K_1 V)}} \left[\frac{1}{2}\sinh 2u_2 - u_2\right] \tag{A.12}$$

Replacing u_2 by u, we get

$$\int_{x_1}^{x_2} dx|p(x)| = (2m^*)^{\frac{1}{2}} \frac{W_1 E_{rel}}{\sqrt{q(V_{b1} - K_1 V)}} \left[\frac{1}{2}\sinh 2u - u\right] \tag{A.13}$$

Hence the quantum transmission probability P_T is given by

$$P_T = \left[\exp\left\{ \frac{(2m^*)^{\frac{1}{2}} W_1 E_{rel}}{\hbar\sqrt{q(V_{b1} - K_1 V)}} \left(\frac{1}{2}\sinh 2u - u \right) \right\} + \frac{1}{4}\exp\left\{ -\frac{(2m^*)^{\frac{1}{2}} W_1 E_{rel}}{\hbar\sqrt{q(V_{b1} - K_1 V)}} \left(\frac{1}{2}\sinh 2u - u \right) \right\} \right]^{-2} \tag{11}$$

where $u = \cosh^{-1}\sqrt{\dfrac{q(V_{b1} - K_1 V)}{E_{rel}}}$.

Appendix B:

Derivation of effective barrier width W_B

The width of the barrier that is seen by an electron as it tunnels through the barrier is given by $x_2 = x_1 = W_B$, where x_2 and x_1 are classical turning points of the tunneling electron and W_B is called effective barrier width (Fig. 4.9). From eqn. (A.3), we get

$$\frac{y_1}{y_2} = \frac{x_1^2}{x_2^2} \tag{B.1}$$

Here $x_2 = W_1$, $y_2 = q(V_{b1} - K_1 V)$, and $y_1 = E_{rel} = q(V_{b1} - K_1 V) - \Delta E_C + E_{th}$.

Hence, $$x_1 = \sqrt{\frac{y_1}{y_2}}\, x_2 = \sqrt{\frac{q(V_{b1} - K_1 V) - \Delta E_C + E_{th}}{q(V_{b1} - K_1 V)}}\, W_1 \tag{B.2}$$

So the effective barrier width is given by

$$W_B = x_2 - x_1 = W_1\left\{ 1 - \sqrt{\frac{q(V_{b1} - K_1 V) - \Delta E_C + E_{th}}{q(V_{b1} - K_1 V)}} \right\} \tag{16}$$

References

[1] B. O' Regan and M. Gratzel, *Nature* **353** (1991) 737.

[2] M. K. Nazeeruddin, A. Kay, I. Rodicio, R. Humphry-Baker, E. Muller, P. Liska, N. Vlachopoulos and M. Gratzel, *J. Am. Chem. Soc.* **115** (1993) 6382, and references therein.

[3] K.M. Krishna, M. Sharon, M.K. Mishra and V.R. Marathe, *Chem. Phys.* **163** (1992) 401.

[4] S.M. Sze, *Physics of Semiconductor Devices*, 2nd Edition, Wiley & Sons, Inc., USA (1981) pp. 255 - 258.

[5] K.W. Boer, *Solar cells* **16** (1986) 591.

[6] H.O. Finklea, in *Semiconductor Electrods,*. H. O. Finklea (ed), Elsevier Science Publishers B. V., Amsterdam, The Netherlands (1988).

[7] H.J. Moller, *Semiconductors for Solar Cells*, Artech House Press, Boston (1993).

[8] C. Goradia and M. Ghalla-Goradia, *Solar Cells* **16** (1986) 611.

[9] A. L. Fahrenbruch and R.H. Bube, *Fandamentals of Solar Cells*, Academic Press, New York (1983).

[10] S.M. Sze, *Physics of Semiconductor Devices*, 2nd Edition, Wiley & Sons, Inc., USA (1981) pp. 800 - 805.

[11] Iwo Bialynicki-Birula, *Theory of Quanta*, Oxford Univ. Press (1992).